Article accepted for publication in the journal Nature Sustainability
https://doi.org/10.1038/s41893-019-0307-1

Article

Potential contributions of pre-Inca infiltration infrastructure to Andean water security

Authors

Boris F. Ochoa-Tocachi[1,2,3,*], Juan D. Bardales[2,4], Javier Antiporta[2,5], Katya Pérez[2,5], Luis Acosta[2,4], Feng Mao[6], Zed Zulkafli[7], Junior Gil-Ríos[2,4], Oscar Angulo[2,4,8], Sam Grainger[9], Gena Gammie[10], Bert De Bièvre[2,11], and Wouter Buytaert[1,2]

Affiliations

1. Imperial College London, Department of Civil and Environmental Engineering & Grantham Institute – Climate Change and the Environment, London SW7 2AZ, UK
2. Regional Initiative for Hydrological Monitoring of Andean Ecosystems (iMHEA), Lima 15047, Peru
3. Institute for Applied Sustainability Research, Quito 170503, Ecuador
4. Superintendencia Nacional de Servicios de Saneamiento (SUNASS), Gerencia de Regulación Tarifaria, Lima 15073, Peru
5. Consorcio para el Desarrollo Sostenible de la Ecorregión Andina (CONDESAN), Lima 15047, Peru
6. University of Birmingham, School of Geography, Earth and Environmental Sciences, Birmingham B15 2TT, UK
7. Universiti Putra Malaysia, Department of Civil Engineering, Serdang 43400, Malaysia
8. Pontificia Universidad Católica del Perú, Departamento Académico de Ciencias Sociales, Lima 15088, Peru
9. University of Leeds, School of Earth and Environment, Leeds LS2 9JT, UK
10. Forest Trends, Washington, DC 20036, USA
11. Fondo para la Protección del Agua (FONAG), Quito 170509, Ecuador

*corresponding author(s): Boris F. Ochoa-Tocachi (boris.ochoa13@imperial.ac.uk)

Abstract

Water resources worldwide are under severe stress from increasing climate variability and human pressures. In the tropical Andes, pre-Inca cultures developed nature-based water-harvesting technologies to manage drought risks under natural climatic extremes. While these technologies have gained renewed attention as a potential strategy to increase water security, limited scientific evidence exists about their potential hydrological contributions at catchment scale. Here, we evaluate a 1,400-year-old indigenous infiltration enhancement system that diverts water from headwater streams onto mountain slopes during the wet season, to enhance the yield and longevity of downslope natural springs. Infiltrated water is retained for an average of 45 days before resurfacing, confirming the system's ability to contribute to dry season flows. We estimate that upscaling the system to the source water areas of the city of Lima can potentially delay 99 million m^3 yr^{-1} of streamflow and increase dry season flows by 7.5% on average, which may provide a critical complement to conventional engineering solutions for water security.

Key words: nature-based solutions | natural infrastructure | indigenous knowledge | ecosystem services | water harvesting

Water stress in the Anthropocene is not only climate-induced[1,2,3]. Effective water resource management needs to consider the interactions between climate variability, water demand, land use, ecological requirements, and socio-political conditions, exacerbated further by uncertainties related to climate change and developmental pathways[4,5,6]. This situation calls for robust and flexible adaptation strategies that require a rethinking of existing strategies to achieve water security. The limitations of solutions based on 'grey' infrastructure, such as artificial reservoirs, are increasingly becoming clear, e.g., high sunk costs, complex planning and implementation, and limited adaptive capacity. This has brought a renewed interest in nature-based solutions or 'green' infrastructure, which can be implemented gradually, adjusted after implementation, and provide multiple benefits that make them highly compatible with climate change adaptation in an increasingly uncertain and complex world[7].

The uptake of nature-based solutions is particularly high in Latin America, where growing investment in catchment interventions and source-water protection schemes aim to optimise the range of ecosystem services provided by catchments while striving for maximum cost-efficiency and flexibility[8]. However, limited quantitative hydrological evidence exists about the impact of various types of interventions on the hydrological processes[9], which is needed to incorporate them in an effective catchment-scale water resource management strategy. This is especially the case for pre-Inca infiltration enhancement systems, a type of indigenous infrastructure that was once widespread and is receiving increasing attention from conservation organisations and policy-makers[10]. The systems are locally known as *mamanteo*[11] —Spanish for *breastfeeding*— or *amunas*[12] —Quechua for *retaining*— and consist of diverting water from natural streams during the wet season to enhance infiltration in mountain slopes. Water delayed by a longer subsurface residence time increases yield and longevity of downslope springs during the dry months.

Here we describe and quantify the hydrological functioning of a 1,400-year-old infiltration system in the Andean highlands near Lima. It was recently restored by a local community to cope with the extreme seasonal and inter-annual hydrological variability and is one of the few remaining active systems of this kind in Peru. We implemented hydrological monitoring and dye-tracer experiments to quantify the system's water storage and delay capacities to bridge dry periods. We find a clear hydrological connectivity between the infiltration canals and downslope springs with a residence time between 2 weeks and 8 months and an average of 45 days. We then simulate the upscaling of the system to the main water source area of the downstream city of Lima, to evaluate whether it can complement the currently installed grey infrastructure and increase Lima's water security. Our findings are essential to design nature-based solutions that increase the reliability of water supply in highly seasonal and arid environments and improve water security and climate change adaptation in mountain regions.

Indigenous water harvesting practices

The lands over which Indigenous Peoples exercise traditional rights are globally important for the conservation of ecologically valuable landscapes and ecosystems[13]. Among local management traditions, practices that cope with water stress have used or revived the use of ancient and nature-based knowledge. For example, groundwater harvesting using sloping tunnels and water wells (known as *qanats*) are widespread in northern Africa and the Middle East[14]. In the western Rajasthan region of India, *paar* systems collect percolated rainwater through sandy soil[15]. In Easter Island, Chile, the location of megalithic platforms (*ahu*) is explained by distance from freshwater sources[16], particularly coastal seeps, where ancient constructions including trenches and impoundments provided a constant source of low salinity water and enabled local inhabitants to survive in drought periods and build the giant

anthropomorphic statues (*moai*)[17]. In mountain regions worldwide, diverting river water to permeable areas through irrigation canals and infiltration zones is a common practice; the *careo* system constructed in Spain during the 9th–15th century by the Arabs[18,19] shares many similarities with the *amunas* developed by pre-Inca cultures in Peru, Chavín initially and Wari later, from as early as the 5th century (Supplementary Table 1). Similar water harvesting structures were found in Machu Picchu[20], where the local hydrogeology generates a lag time of several months between rainfall and discharge[21]. These approaches have been based upon tacit community knowledge of local hydrological processes. More recently, they are attracting renewed interest from national-level policy makers in Latin America as a potential means to address urban water supply challenges and to implement the Sustainable Development Goals[7,10,22].

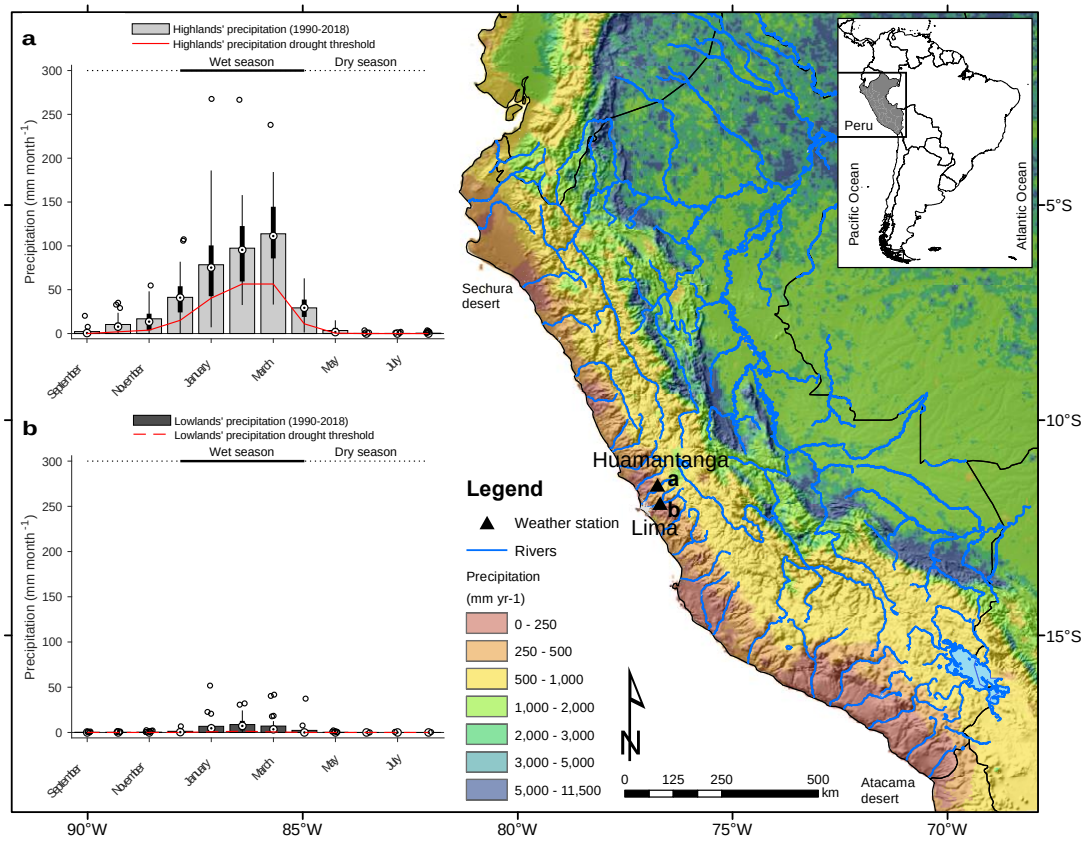

Fig. 1 | Spatiotemporal variability of precipitation in the Peruvian Andes. Mean annual precipitation climatology (1998–2014)[23]. The inset plots show monthly precipitation (1990–2018), **a**, in Lima's highlands (Huamantanga station, 11°30'0.0" S, 76°45'0.0" W, 3392 m a.s.l.) and, **b**, close to Lima city (Chosica station, 11°55'47.5" S, 76°41'22.8" W, 863 m a.s.l.). Bars represent the mean, target symbols show the median, black boxes are limited by the 25th and 75th percentiles in monthly precipitation, whiskers correspond to ±2.7σ and extends to the adjacent data value that is not an outlier, and outliers are shown as white circles. Red lines in all plots represent drought conditions using a variable threshold level approach[64,65], based on a 30-day moving average method and defined at the 20th percentile of inter-annual data from 1990 to 2018. During this period, the average annual rainfall in the Huamantanga station was 380.3±139.0 mm, and 25.9±22.7 mm in the Chosica station. Precipitation seasonality is a strong determinant of the hydrological regime of rivers that supply water to the arid Pacific coast of Peru, with most of the streamflow originating from precipitation in the highlands.

This is the case in the Pacific slopes of the Central Andes, where achieving water security is particularly challenging (Fig. 1). The interaction between various synoptic-scale climate processes and the complex Andean topography create extreme spatial and temporal gradients in precipitation[23]. During the South American monsoon season (austral summer), warm and moist air transported from the tropical Atlantic by mid-level easterly winds over the Amazon basin are blocked by the Andes, causing pronounced orographic effects and a strong altitudinal precipitation gradient[24,25]. The meridional displacement of the Intertropical Convergence Zone (ITCZ) over the eastern Pacific induces a strong seasonal variability,

concentrating precipitation over the Andes of southern Ecuador and northern Peru during the austral fall, when the ITCZ reaches its southernmost position[26]. In addition, the presence of the cold Humboldt Current and the subtropical anticyclone over the southeast Pacific Ocean generate arid and stable conditions between the Atacama Desert in northern Chile and the Sechura Desert in northern Peru that penetrate the Andean western slopes[27]. At interannual timescales, El Niño-Southern Oscillation (ENSO) is the major driver of precipitation variability[23,28]. Only during warm ENSO conditions, precipitation decreases over northern South America whereas it increases over subtropical South America and along the arid Peruvian coast, with the opposite effects during cold ENSO conditions[26].

The arid coastal region of Peru is home to 60% of the country's population. It relies on surface water resources originating in the Andes to supply water for large-scale irrigated agriculture, industry, and domestic use for the coastal regions including Peru's capital Lima[29]. Andean rivers are characterised by fast hydrological responses, prone to flash floods during the wet season and low to non-existing base flows during the dry season. This variability is exacerbated by the impact of human activities, in particular soil degradation and land use change[30,31], trends of increasing seasonality of precipitation[32,33], and accelerated glacier melt[34,35]. Because of the seasonal flow regime, large supply-demand deficits occur during the dry season that need to be bridged with artificial storage. For example, Lima currently experiences a water deficit of approximately 43 $x10^6m^3$ during the dry season[36] (Supplementary Fig. 1), and depends on a total artificial storage capacity of approximately 330 $x10^6m^3$, along with hundreds of natural springs, lakes, glaciers, and wetlands[37].

From as early as 600 AD, pre-Inca communities developed catchment interventions to increase water availability during the dry season in response to the naturally variable flow regime[38,39]. We studied one of the last remaining infiltration systems located in the agro-pastoralist community of Huamantanga at an elevation of 3,300 m a.s.l. in the central Peruvian Andes (Fig. 1 and Supplementary Fig. 2). Local livelihood activities, which consist of raising livestock for cheese production and irrigated agriculture for subsistence, heavily depend on seasonal river flows[40,41]. The infiltration system is designed to increase available water for irrigation during the dry season and consists of the following elements (Fig. 2 and Supplementary Fig. 3):

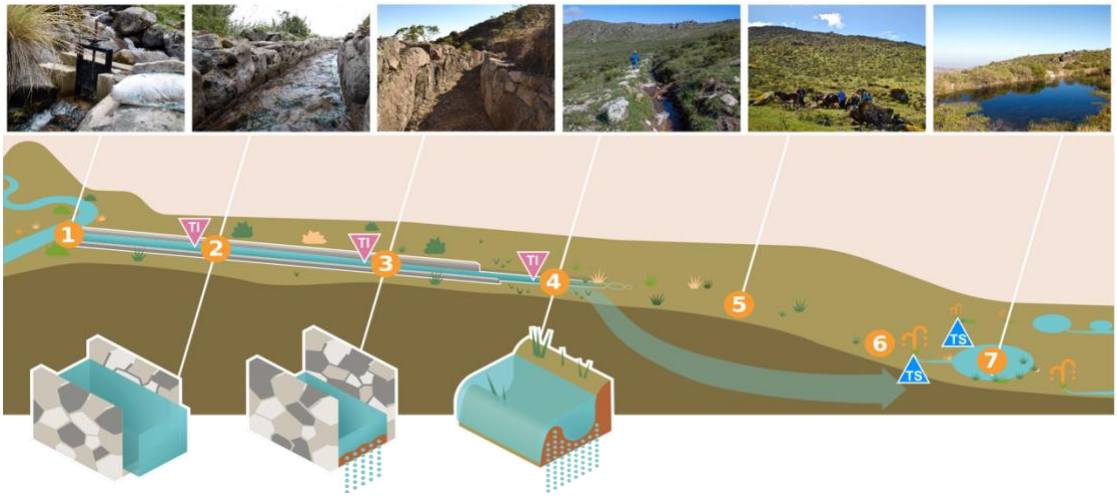

Fig. 2 | Conceptual model of the pre-Inca infiltration enhancement system. Features of the system: diversion canals (1 and 2), infiltration canals (3 and 4), infiltration hillslopes (5), springs (6), and ponds (7). Tracer injection (TI) and sampling (TS) points are marked schematically in the diagram.

- *Diversion canals:* Typically impermeable structures of two types: (i) long canals that divert wet season flows from small streams to infiltration canals and hillslopes, and (ii) short canals that route excess water to ponds, or from ponds to other streams downslope.

- *Infiltration canals:* Earthen canals and ditches that transport water further towards the infiltration hillslopes while simultaneously allow infiltration into the subsurface. At this point, up to 30 ancient infiltration canals have been identified in Huamantanga[11], of which 11 are still in operation. The remaining were either abandoned or clogged.
- *Infiltration hillslopes:* Rocky or stony areas that receive water from canals and ditches and spread it in the field. The fractured nature of the rocks allows water to infiltrate, enhancing recharge to subsurface stores and delaying water leaving the catchment through subsurface flow.
- *Springs:* These are typically natural occurrences that are enhanced by the resurfacing of infiltrated water. We mapped 65 active springs during the wet season, most of which discharge all year according to local testimonies.
- *Ponds:* Small water bodies (around 300 m^3 each) that are used to regulate the flow through the infiltration system. They serve two purposes: (i) to store water for direct access, and (ii) to enhance further subsurface water infiltration. We found 14 ponds currently functioning and vestiges of up to 30 abandoned ponds.

Two main mechanisms delay runoff. First, spreading the water in the hillslopes enhances infiltration, which increases subsurface storage and delayed discharge in the downslope springs. A considerable number of active and extinct springs located downslope of the infiltration areas gives evidence of this (Fig. 3a). Second, the system creates surface storage in ponds fed by streams, canals, and springs that can either be used directly or enhance further infiltration. Various configurations exist, including repeated resurfacing, harvesting, and cascading infiltration of water along a hillslope (Fig. 3b).

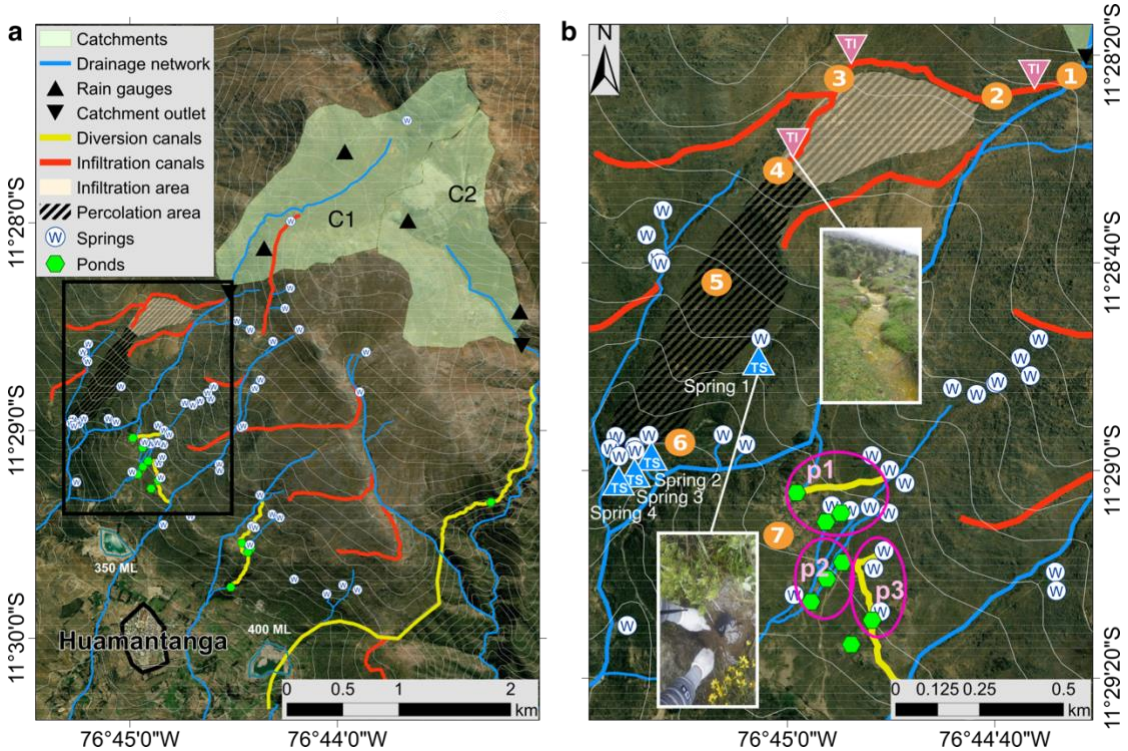

Fig. 3 | Spatial distribution of the infiltration system and monitoring experiments. a, Spatial distribution of the elements in the infiltration system, which indicates an indigenous knowledge about the underlying hydrological processes. The monitored catchments C1 and C2 (green) are located immediately upstream of the system intakes. **b**, Detail of the evaluated infiltration system, location of the tracer injection (TI) and sampling (TS) points in the field, and distribution and functioning of ponds (bottom right): **p1**, Some ponds receive surface water flow directly from streams or from other ponds. The flow routing finishes when water discharges to a larger stream. **p2**, Ponds constitute a series of cascading elements that delay the flow of water downslope. The delayed water can either re-infiltrate to the subsurface or overflow to other ponds. **p3**, Some ponds receive subsurface water flow from springs, which enhances further the hydrological regulation. Base map sources: Esri, DigitalGlobe, Earthstar Geographics, CNES/Airbus DS, GeoEye, USDA FSA, USGS, Aerogrid, IGN, IGP, and the GIS User Community.

Results

We injected a dye tracer (eosin) into a diversion and infiltration canal upslope and monitored its emergence in downslope springs using activated carbon samplers. Our experiments reveal a clear hydrological connectivity between the canal and the springs, with a mean residence time of the dye tracer of 45 days, ranging from 2 weeks to 8 months (Fig. 4c, Supplementary Table 2, and Supplementary Fig. 4). These results show that the system can store wet season flow effectively and recover it during at least a part of the dry season. The variability in residence times and resurface concentrations between springs can be related to spatial heterogeneity and preferential flow pathways of the subsurface. Preferential flow pathways may be responsible for early tracer emergence, whereas water in deeper soil layers might remain longer in the subsurface while it replaces old water[42,43]. The slight increase in tracer concentration in springs 1 and 3 in September and October (Fig. 4c) can be attributed to replacement water from small rainfall events announcing the start of the next wet season (Figs. 4a and 4b).

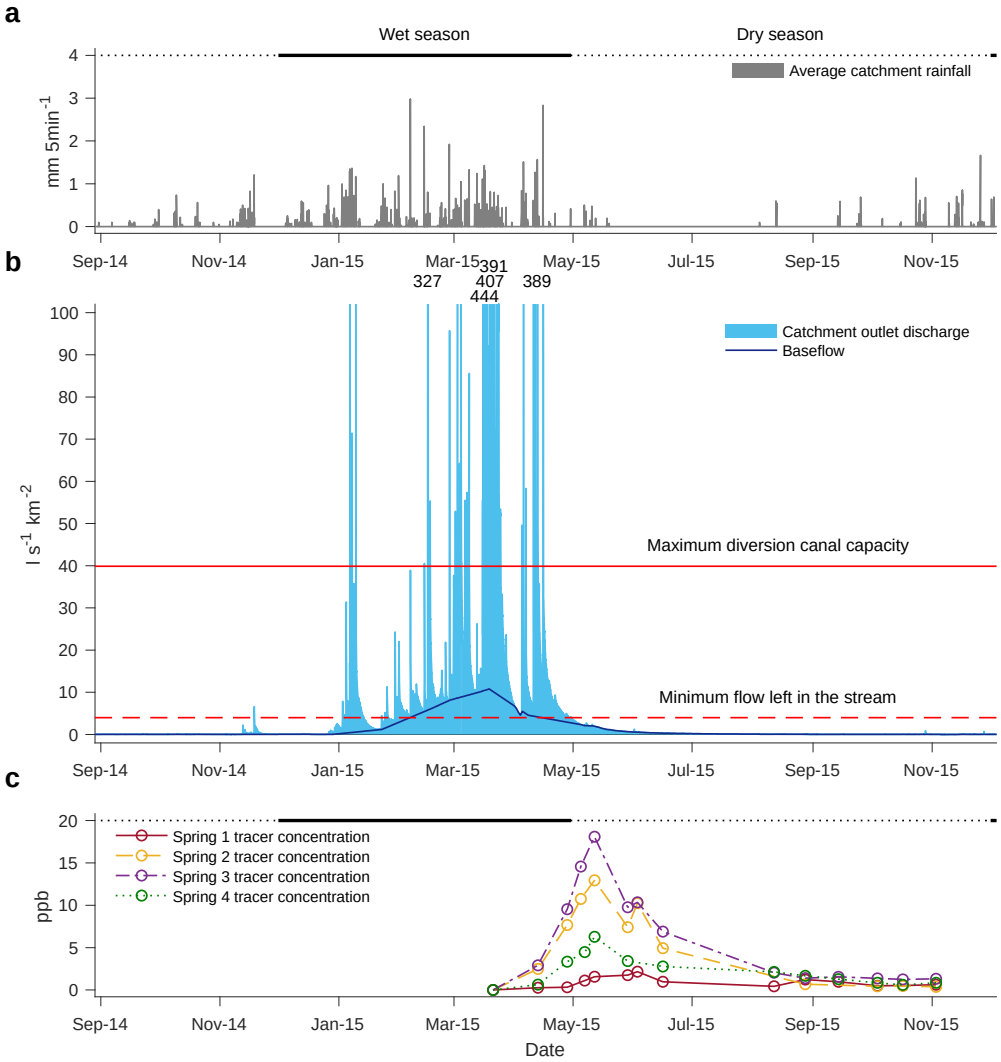

Fig. 4 | Time series of rainfall, streamflow, and tracer emergence in springs. Data from catchment C1 during 2015 is shown in the figure. **a,** High-resolution precipitation time series. The span of the wet and dry seasons is indicated by the bold and dotted black lines, respectively. **b**, High-resolution discharge time series (light blue), baseflow (dark blue), minimum flow to initialise diversion (dashed red line, 4 l s^{-1} km^{-2}), and maximum diversion canal capacity (continuous red line, 39.9 l s^{-1} km^{-2}). The axis is cut at 100 l s^{-1} km^{-2} to improve readability of the variable flow regime. Peak magnitudes in excess of 300 l s^{-1} km^{-2} are displayed above the axis. **c**, Eosin concentrations in four springs located downslope of the diversion canal in C1. After tracer injection on March 21, 2015, the first sample reveals that some water had resurfaced within the following 23 days; the maximum

emergence occurred in May, two months after the injection; followed by a progressive decline in concentrations without completely disappearing until the end of the monitoring period, eight months later.

To quantify potential infiltration volumes, we implemented hydrological monitoring in two headwater catchments (C1 and C2) whose outlets are located immediately upstream of the system intakes. During the hydrological years 2014–2015 and 2015–2016, rainfall in catchments C1 and C2 averaged respectively 563 mm yr^{-1} and 528 mm yr^{-1} with a clear monomodal seasonality (Fig. 4a). River discharge reflects this seasonality (Fig. 4b) and yielded runoff ratios (ratio between annual discharge and annual precipitation) of respectively 23.66% and 21.22%. The discharge generated during the wet season accounts for most of the total annual discharge in the monitored catchments (Table 1). This yields a water volume between 83.9 and 170.2 $x10^3 m^3 km^{-2}$ that is available for potential diversion to the infiltration system. In comparison, the community of Huamantanga currently operates two reservoirs with design capacities of 350 and 400 $x10^3 m^3$ to store water for irrigation (Fig. 3a). Although the short residence time implies that the infiltration system is unable to replace artificial storage, it can potentially provide additional storage capacity to complement the existing grey infrastructure. This complementarity depends on the recovery rate of the system.

Table 1 | Annual water balance, and potential and actual flow diversion from the monitored catchments (C1 and C2) during the wet season.

	Annual water volumes		Wet season flow diversion	
Catchment (area) [km^2]	Rainfall [mm]	Discharge [mm]	Potential [mm]	Actual [mm]
C1 (2.09)	536.2–606.8	89.7–176.9	83.9–170.2	33.2–95.7
C2 (1.69)	494.8–568.7	98.8–125.5	92.1–115.9	51.3–75.5

Minimum and maximum volumes are given. A volume of 1 mm equals 1000 m^3 km^{-2}. The hydrological year in the study region runs from 01 September to 31 August. The wet season runs from 01 December to 30 April (Fig. 4). The actual diversion is determined by the hydraulic design of the diversion system and is typically lower than the potential diversion, which is determined by the discharge during the wet season and environmental flow requirements.

The actual volume of diverted water tends to be lower than the potential volume because of the system's hydraulic capacity and operational restrictions. The intake capacity is determined by the dimensions of the abstraction gate and canal (Fig. 2), which are typically constructed smaller than the maximum flow of the wet season. The maximum capacity of the studied infiltration canal is 75 l s^{-1} despite peak river flows of up to 930 l s^{-1}. Also, typically less than 100% of the available streamflow is diverted to keep a minimum ecological flow for environmental purposes and other downstream water uses[44]. We estimated this flow at 4 l s^{-1} km^{-2}, which is the long-term average flow in the monitored catchments (Fig. 4b). This results in actual diverted volumes between 33.2 and 95.7 $x10^3 m^3 km^{-2}$, depending on the total seasonal rainfall volume (Table 1), and represents approximately 54% of the wet season discharge. We estimated a recovery rate of 0.5, resulting of subtracting losses from evapotranspiration and deep percolation that bypasses the downslope recovery springs. Using these values, we find that the infiltration system can increase natural dry season flow of the local stream between 3% to 554% (Supplementary Fig. 5).

Using the hydrological characteristics of the Huamantanga infiltration system, we then investigated whether upscaling it to the main source water areas of Lima, in the Rimac river basin, can contribute to the city's water supply. We identified 1,428 km^2 of highlands whose elevation is above 4,000 m a.s.l. (Supplementary Figs. 2 and 6). This area has a mean annual rainfall climatology[23] of 505 mm, of which 410 mm (81%) fall during the wet season (Supplementary Table 4). The contributing area of the Rimac basin to the Chosica station is 2,319 km^2, with a mean annual rainfall climatology of 437 mm, of which 364 mm fall during the wet season. Using the mean runoff ratio obtained for Huamantanga of 22%, and assuming a diversion capacity of 50% of the wet season discharge in the highlands –in line with the actual diversion rate of 54% of the Huamantanga system–, we calculate that 34.7% of the Rimac river wet season discharge can potentially be diverted. This figure represents a volume of 198

$x10^6m^3yr^{-1}$, out of an average Rimac river discharge measured at the Chosica station of 972 $x10^6m^3yr^{-1}$[37]. Applying the residence time distribution obtained for the Huamantanga system and conservatively assuming an effective recovery rate of 0.5, we obtain an average increase in dry season flow for the Rimac river of 33% at the start of the dry season, reducing to less than 1% at the end of the dry season (Fig. 5 and Supplementary Fig. 7). The initial reduction in monthly discharge at the beginning of the wet season is the result of more water being taken out than returned to the river in that month. In practice, the operation of the indigenous infrastructure could be adjusted with the operation of the modern infrastructure in place (Supplementary Fig. 8).

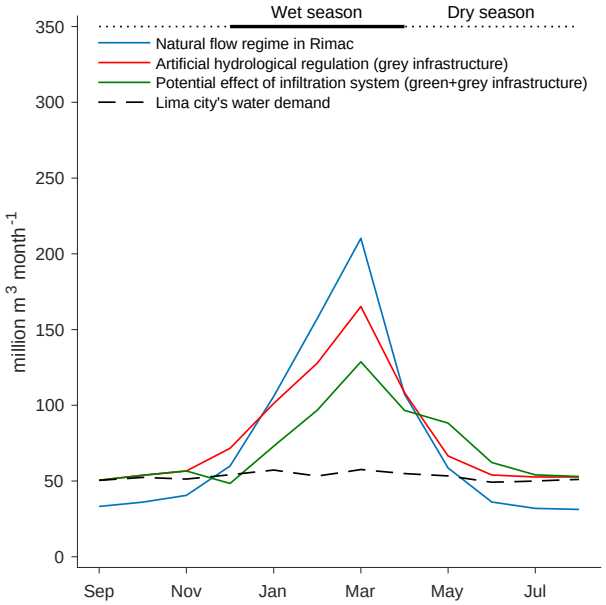

Fig. 5 | Potential contributions of pre-Inca infiltration infrastructure to Lima's water supply. The natural flow regime of the Rimac river (blue) is estimated from records covering the period 1921–1960. From 1960, the effect of grey infrastructure is evidenced by its artificial hydrological regulation effects (red), reducing wet season surplus and increasing dry season flows[37]. The potential effect of upscaling pre-Inca infiltration infrastructure (green) is estimated on top of that of the grey infrastructure. Estimated diverted flows are calculated using long-term daily river flow records for the Rimac river (1961–2018), residence times are calculated from the normalized tracer concentrations scaled by the estimated spring flow (Supplementary Fig. 4), the recovery rate is estimated in 0.5, and modified flows are subsequently accumulated at monthly scale. Interannual variability is represented by the shaded areas using the 5th and 95th percentiles of monthly data. The dashed line represents Lima's total water demand[36].

Given the current levels of water stress, the estimated amounts can provide a critical contribution to Lima's water supply. Rainfall in the lower part of the catchment is negligible (Fig. 1 and Supplementary Table 6), thus groundwater and dry season baseflows are predominantly replenished by highland precipitation and interbasin transfers[45]. Since 1960, the natural flow regime of the Rimac river has been modified with a range of civil infrastructure to increase its hydrological regulation capacity[37] (Fig. 5). Because of the subseasonal residence time of the infiltration systems, it is not possible to replace artificial storage systems entirely. However, the increased baseflow during the dry season can make existing infrastructure more efficient and increase their capacity to buffer short drought spells (Supplementary Table 7). This could allow serving a higher water demand with the same infrastructure. Furthermore, the recovery rate may be larger at a regional scale compared to the local scale, as some of the water may resurface further downstream and replenish groundwater aquifers at the coast that can be exploited[46]. A sensitivity analysis for the recovery rate (0.4–0.7) and associated recovered water volumes (79–138 $x10^6m^3yr^{-1}$) and dry season flow increase percentages (6–10%) are presented in the Supplementary Information (Supplementary Table 8 and Supplementary Fig. 7).

Implications for water security

Globally, the sustainability of mountain water resources is threatened by a variety of processes including soil degradation, land use change, changing precipitation patterns, and accelerated glacier melt[30,31,32,33,34,35]. Achieving water security through conventional engineering approaches such as dams and reservoirs involves considerable logistical, financial, engineering, and environmental challenges. These approaches require long-term investment and political stability. However, concerns have been raised about their capacity to adapt to uncertain future hydro-climatic and demographic trends. Because of the large and acute pressure on water resources, several Andean countries have become a testbed for approaches that complement traditional solutions with a wider set of catchment interventions that leverage natural processes[47]. The uncertainties in future projections of precipitation and water availability complicate the design of large, fixed infrastructure with a long lifespan. The flexibility of natural infrastructure, which can be implemented and expanded more gradually and adjusted in line with future changes in climate conditions, is therefore seen as a promising way to enhance the adaptive capacity of water resource systems[7,22].

For this reason, Peru's drinking water regulator SUNASS is currently incentivising and supporting public water utilities of Lima and other cities to complement traditional engineering infrastructure with nature-based solutions for source-water protection[48]. Peruvian water utilities, including SEDAPAL of Lima, have responded by designing and implementing a portfolio of catchment interventions, which is funded by a water tariff regulated by SUNASS. A recent Law on Reward Mechanisms for Ecosystem Services (2014)[8] provides the legal framework and establishes permissible interventions. It also puts strong emphasis on the integration of scientific and indigenous knowledge, including the rehabilitation of water harvesting infrastructure such as the described infiltration enhancement systems[10]. This has led to an increasing need to quantify the potential hydrological benefits of these practices, and to identify explicitly the beneficiaries as a prerequisite to combine grey and green infrastructure and to maximise the cost-benefit ratio in the context of water supply and drought resilience.

Identifying which combination of interventions optimises the return-on-investment and adaptive capacity in view of future climate uncertainty remains a challenge, especially in mountainous regions. It is expected that mountains will experience stronger warming than lowlands[32,35], which makes them particularly prone to having negative impacts on water resources, including the loss of water regulation capacity in high Andean wetlands, and accelerated retreat of glaciers[49,50]. Similarly, climate change is modifying the ecological boundaries and processes of other Andean biomes[51], with potentially serious impacts on water resources. The implementation of adequate adaptation strategies will need to respond to these changes, as well as a growing anthropogenic demand for water[52]. Increasing natural and artificial water storage and hydrological regulation in catchments is a robust adaptation strategy. Our results show that the development of solutions that integrate elements of indigenous practices and nature-based solutions can play a role in this.

In practice, infiltration systems will have to be part of a more integrated catchment-scale water management strategy. Historically, this has included grassland conservation, headwater protection and sustainable grazing, water harvesting methods, terrace building on lower climatic zones for sustainable agriculture and erosion control, aqueducts to abstract and transport groundwater in the coastal region, and irrigation systems using earthen canals to increase aquifer recharge and promote water use efficiency. Given the current water stress pressure, this study provides the scientific evidence needed to upscale indigenous infrastructure, thus challenging the preconception that local water management traditions are outdated and supporting the uptake of nature-based solutions for water security.

Conclusions

We combined hydrological monitoring and tracer experiments to characterise the hydrological functioning of a 1,400-year-old infiltration enhancement system developed by pre-Inca cultures to cope with climate variability in the Peruvian Andes. Our results confirm that the system effectively enhances hillslope infiltration to reach downslope springs. We estimate a mean residence time of 45 days, with a range between 2 weeks and 8 months, which shows that the system can be used to increase water availability at the community scale during the dry season. This is in line with its original use, which is to extend the wet season successfully and allow for longer crop-growing period for local farmers. However, its potential to improve water supply at a regional scale was thus far unknown. Using similar parameters that control the system in Huamantanga and conservative assumptions about the recovery rate of the infiltration system and land suitability for its replication, we estimate that the practice can divert and infiltrate approximately 35% of the wet season flow of the entire Rimac basin (198 million m^3 yr^{-1}, recovering 99 million m^3 yr^{-1}) and increase the basin dry season volumes by 7.5% on average and up to 33% during the early dry months. The subseasonal residence times of the system need to be combined with classic engineering storage solutions to increase water security for downstream rural and urban users. Such combination can increase their cost-benefit ratio and performance, in particular, to bridge short drought episodes.

Further hydrological characterisation is necessary to implement similar indigenous infrastructure and nature-based solutions as part of an integrated catchment-scale water resource management strategy. In particular, better understanding of the physiographic and hydrological controls on residence time distribution and recovery rate can improve the accuracy of estimating potential contributions at basin scale. Furthermore, recovery rates at different spatial scales are currently unknown, and depend on the local geology, as well as connectivity and exploitability of subsurface aquifers. Nevertheless, the restoration of the Huamantanga system has triggered an interest in nature-based solutions for water security in the region. Our results show that revaluing indigenous knowledge, practices, and systems can complement scientific and engineering options to contribute to the major challenge of supplying water to large urban populations in hydrologically variable and arid environments, and thus to improve their water security and climate resilience.

Methods

We used a combination of participatory mapping, hydrological monitoring, dye-tracer experiments, and hydrological modelling to characterize and quantify the storage and regulation capacity of a pre-Inca infiltration enhancement system. We then estimated the potential local and regional effects of upscaling this system to contribute to water supply in the arid coastal plain.

Participatory mapping. Focus group discussions, interviews, and surveys were conducted within a group of 117 community members (‘comuneros’) to access their knowledge of their ancient practices and to record their field experiences in relation to the operation and maintenance of the infiltration system[41,53,54]. Three main methods were used to collect data: (i) semi-structured interviews, including a list of guiding questions yet flexible enough to follow the conversation with the interviewed person; (ii) group discussions with key people who were invited to converse about a predefined topic and, occasionally, with additional people who attended the meetings as they were open; and, (iii) observations in which we joined certain daily activities (sometimes by invitation, and others by request), to observe the local dynamics and ask questions when possible. Details and participants of 57 interviews, 11 workshops, 8 observations, and 5 local visits are indicated in Supplementary Table S9. A survey of physical features generated relevant geographical information of the system components that were depicted in posters drawn by local community members (Supplementary Fig. 3),

which were subsequently mapped in the field and digitised (Fig. 3). The system was mapped, reconstructed, and monitored together with comuneros as part of a broader research project on adaptive governance of mountain ecosystem services for poverty alleviation[55], and in line with multiple governmental and non-governmental interventions.

Dye-tracer experiments. We injected 907 g of eosin (Acid Red 87) in the Pacchipucrio canal (flowing out of catchment C1, Fig. 3). The downslope springs were equipped with activated carbon samplers, which contain 4.25 g of Barnebey and Sutcliffe Type AC Activated Carbon with a surface area of 1,150 $m^2\ g^{-1}$[56]. The samplers were retrieved at variable time intervals for operational reasons (Supplementary Table 2) and analysed in the Ozark Underground Laboratory to quantify the amount of accumulated tracer. Following its protocol[56], 15 ml of a standard elution solution were used for each carbon sampler, consisting of a mixture of 5% aqua ammonia and 95% isopropyl alcohol solution and sufficient potassium hydroxide pellets to saturate the solution. The isopropyl alcohol solution is 70% alcohol and 30% water. The aqua ammonia solution is 29% ammonia. The dye concentrations are calculated by separating fluorescence peaks due to dyes from background fluorescence on charts, and then calculating the area within the fluorescence peak. This area is proportional to areas obtained from standard solutions. Detection limits of eosin are 0.008 ppb in water and 0.035 ppb in elutant. Dye quantities are expressed in mg l^{-1} or ppb (parts per billion) accumulated during the period that the samplers stayed in the field. These data were converted into time series by assuming a linear accumulation rate of the dye tracer over each sampling interval (Fig. 4c and Supplementary Fig. 4). We use the tracer concentration in the elutant as proxy for the tracer concentration in the spring water.

Hydrological monitoring and potential infiltration volumes. Precipitation and streamflow were measured from June 2014 to January 2017 at high temporal resolution in two headwater catchments (C1: 2.09 km^2, and C2: 1.69 km^2) that feed the infiltration system intakes (Fig. 3). The catchments are part of the Regional Initiative for Hydrological Monitoring of Andean Ecosystems (iMHEA)[57]. Precipitation was measured in each catchment using two tipping bucket rain gauges of 0.2 mm resolution installed at a height of 1.50 m above ground and distributed at low and high elevations to consider precipitation altitudinal gradients. We applied a cubic spline interpolation algorithm[57] on the rainfall observations to generate time series at a 5-min interval, which were then averaged per catchment and aggregated at daily and monthly scale (Fig. 4a). Streamflow was calculated as a function of water level, for which we used sharp-crested weirs with a combined 90°-V-notch and rectangular section. Water level measurements were taken at a regular interval of 5 min using vented-tube pressure transducers with nominal sensor resolution of 0.01 cm H_2O (0.0034 FS) and accuracy of ±0.12 cm H_2O (±0.06 FS). In addition, we obtained daily rainfall data from the National Hydrology and Meteorology Service of Peru (SENAMHI) in Huamantanga (1964–2018) and Chosica–Lima city (1990–2018), and river flow data from the National Water Authority of Peru (ANA) in Chosica–Rimac river (1920–2018)[37].

Water volumes shown in Table 1 were calculated by summing catchment averaged precipitation and streamflow observations in catchments C1 and C2 for hydrological years 2014–2015 and 2015–2016. The hydrological year ranges from 01 September to 31 August, whereas the wet season ranges from 01 December to 30 April. As the diversion canal intakes of the infiltration system are located immediately downstream of the monitoring weirs, the recorded streamflow time series were used to calculate the potential and actual diverted wet season water volumes shown in Table 1. The minimum flow threshold to start diversion was set at 4 l s^{-1} km^{-2}, which corresponds to the average flow in catchments C1 and C2 during the monitoring period. The maximum diverted flow was based on a diversion canal capacity of 75 l s^{-1} for C1 (2.09 km^2), which on top of the base 4 l s^{-1} km^{-2}, is equivalent to 39.9 l s^{-1} km^{-2} (Fig.

4b). We assume that these characteristics are typical for an infiltration system and therefore use them in the regional model.

Estimation of tracer residence time and construction of the subsurface flow delay function. We used the interpolated time series of tracer concentration in the spring water (Fig. 4c) to estimate the residence time of the infiltrated water in the hillslope and to construct a delay function to use in the regional model. As it was not feasible to measure the discharge of the springs directly, we estimated this discharge at a daily timestep by calculating the baseflow per unit area of monitored catchment C1 using the method of the UK Low Flow Estimation Handbook[58]. This method divides the mean daily flow data into non-overlapping blocks of five days, from which the minima of each consecutive block were computed. The method then searches for turning points in this sequence. Daily baseflow values are calculated by linear interpolation between the turning points and are limited by the original hydrograph when the interpolation exceeds the observations[57]. We then scaled the tracer concentrations by the spring flow at each time step and normalised them to sum 1, in order to use it as a unit hydrograph for the subsurface flow delay at a daily timestep (Supplementary Fig. 4). The unit hydrograph was also interpolated at 5-min resolution to use it at the local scale with the high-resolution streamflow data. The mean residence time τ is given by the first moment of the residence time distribution E(t):

$$\tau = \int_0^\infty tE(t)dt$$

Estimation of recovery rate. We estimated a recovery rate for the artificial infiltration of 0.5, which results from losses incurred by enhanced evapotranspiration from the infiltration zone, and deep percolation bypassing the recovery zone[46]. Shallow subsurface flow that might not enter the infiltration zone but eventually return to the stream is omitted from the losses.

Losses from evapotranspiration are calculated on the area where the diverted water infiltrates into the hillslope (A_i = 0.12 km^2, Fig. 3). Throughout the period that water flows are diverted from the stream and deposited on this area, the soil will be close to saturation. The annual reference evapotranspiration rate (ET_0) for Huamantanga is approximately 902 mm yr^{-1}[40]. Assuming a crop coefficient K_c of 1 (grass reference crop) and no water stress, actual evaporative losses (ET_a) from this area during the 5-month diversion period (from December to April) are estimated in 45.1 x10^3 m^3 yr^{-1}:

$$ET_a = A_i K_c ET_0 \frac{5}{12}$$

which represents 33.5% of the average diverted volume per year (134.6 x10^3 m^3 yr^{-1}, Table 1). We use this value to estimate losses from the artificial infiltration, which is a conservative estimate because it neglects natural evapotranspiration rates that would have occurred without flow diversion taking place.

Losses from deep percolation are calculated considering the geology of Huamantanga, characterised by the Calipuy formation that consists of a mixture of volcanic and sedimentary material[59]. Few groundwater studies are available for this region, but according to Lerner *et al.*[60], upland areas do not contribute greatly to groundwater recharge. This is compatible with the classification of the bedrock as a low-permeable aquitard by the Peruvian Geological Mining and Metallurgical Institute (INGEMMET)[61]. As a conservative estimate, here we use a recharge value of 1 mm d^{-1}, which is distributed equally between the natural rainfall (r_n = 0.5 mm d^{-1}) and the artificial drainage (r_a = 0.5 mm d^{-1}). Owing to the lack of specific studies, this is necessarily an arbitrary value that can be adjusted when more data become available. Combined with the total hillslope area of the infiltration system at Huamantanga (A_h = 0.30

km^2, Fig. 3), this results in a loss of the infiltration water from deep percolation (DP) of 22.8 x10^3 m^3 yr^{-1}:

$$DP = A_h r_a 365 \frac{5}{12}$$

or around 16.9% of the average diverted flow per year. The combined loss of enhanced evaporation and deep percolation is therefore estimated at 0.504 and the recovery rate at 0.496, which is in line with a previous study that assumed a fixed recovery rate of 0.5[62].

Simulation of basin-scale application of artificial infiltration systems on the river flow regime. We developed a computational model to simulate the potential impact on the river flow regime of upscaling the infiltration practice to the entire Rimac river basin, and to compare this impact with that of existing grey infrastructure (see Supplementary Information). The specific characteristics of each system will depend on the local site conditions. Because of the lack of specific regional information, we use the subsurface delay characteristics and intake altitude (4,000 m a.s.l.) of the infiltration system in Huamantanga as representative characteristics for our regional model (Supplementary Fig. 2). Using SRTM elevation data at 1-arc second resolution[63] projected on the Universal Transverse Mercator (UTM) zone 18, the Rimac basin area above 4,000 m a.s.l. was calculated as 1,428.1 km^2 and the contribution area to the Chosica station as 2,318.8 km^2 (Supplementary Fig. 6). Mean monthly precipitation for these areas was estimated using a merged satellite-rain gauge product using a residual ordinary Kriging technique[23] for the period 1998–2014, and the average of the runoff ratios observed in catchments C1 and C2 (22.44%) was applied to the rainfall estimates to calculate runoff volumes (Table 1 and Supplementary Tables 4 and 5). We then assumed that 50% of the total wet season river discharge generated from this area can be diverted into an infiltration system, in line with the actual diversion proportion of 54% of the Huamantanga system (Table 1). We then routed this part of the discharge through the subsurface delay function calculated from the tracer experiment in the Huamantanga system and applying the estimated recovery rate of 0.5. This model was applied to the daily discharge observations of the Rimac at the Chosica station provided by the National Water Authority (ANA). The impact of the infiltration practice on river discharge was compared to two other scenarios: the natural flow regime (1921–1960) and the flow regime modified by the construction of water infrastructure (1960–2018)[37]. Ranges of interannual variability for each month of the year were calculated using the 5th and 95th percentiles of monthly data (Fig. 5 and Supplementary Figs. 1 and 7). Results from a sensitivity analysis for the recovery rate is presented in Supplementary Table 8 and Supplementary Fig. 7.

Drought analysis. Meteorological and hydrological drought was analysed using the threshold level approach[64], in which drought events are identified when the value of the variable falls below a pre-defined threshold. To account for seasonality, we used a variable threshold level based on a 30-day moving average defined at the 20th percentile of inter-annual data[65]. This results in an individual threshold level for every day in the year derived from the cumulative distribution function of the measured variable averaged on that day and the 15 days before and after that day, for all years in the time series. Drought durations were calculated as the total number of consecutive days in which precipitation was below the threshold. Drought events separated less than 10 days were merged together in a single drought event. Short dry spells with a duration of less than 10 days were removed. Deficit volumes were calculated as the sum of the negative precipitation anomalies from the threshold during the drought events. Subsequently, the mean, standard deviation, and maximum were calculated for annual volumes, drought durations, and deficit volumes. For meteorological drought characteristics, we analysed precipitation time series from the Chosica station during the period 1990–2018 and from Huamantanga station during the periods 1964–2018 and 1990–2013 for comparison

(Supplementary Table 6). For hydrological drought characteristics, we analysed the Rimac river flow at the Chosica station during the periods 1921–1960 (natural flow regime), 1961–2018 (altered flow regime as a result of civil infrastructure), and the simulated flows influenced by the infiltration system for 1961–2018 (Supplementary Table 7).

Data availability

Data from the hydrological monitoring of catchments C1 and C2 are described in Ochoa-Tocachi *et al.*[57] and available from Data Citation 1 therein and in the Supplementary Information (Supplementary Data 1). The data consist of the original time series of rainfall and streamflow, and physical characteristics and hydrological indices of the monitored catchments. The data from the dye-tracer experiments are provided in Supplementary Tables 2 and 3. The data from the long-term rainfall stations, Huamantanga and Chosica, and Rimac river flow were provided by SENAMHI and ANA and included here with permission[66] (Supplementary Data 2 and 3).

Code availability

Calculations were implemented using custom code in MATLAB R2018b (version 9.5). The scripts are available on https://github.com/topicster/mamanteo[66].

Additional information

Supplementary information is available for this paper.
Correspondence and requests for materials should be addressed to B.O.T.

Author contributions

B.O.T., B.D.B., K.P., L.A., J.G.R., G.G., and W.B. designed the research approach; B.D.B., K.P., L.A., J.D.B., J.A., J.G.R., and O.A. designed the experiments; J.D.B., J.A., K.P., J.G.R., O.A., F.M., Z.Z., and S.G. performed the experiments and fieldwork; B.O.T., J.D.B., J.A., W.B., and B.D.B. analysed the data; B.O.T. and W.B. developed the modelling approach; W.B., B.D.B., G.G. were principal investigators of research projects that funded this work. B.O.T. and W.B wrote the paper with further contributions from all authors. All authors were involved and participated in the discussion of ideas, read and approved the final version of the manuscript.

ORCID

Boris F. Ochoa-Tocachi: 0000-0002-4990-8429
Juan D. Bardales: 0000-0002-8302-8505
Feng Mao: 0000-0002-5889-1825
Zed Zulkafli: 0000-0001-6271-8593
Oscar Angulo: 0000-0003-0226-5355
Sam Grainger: 0000-0003-0116-5758
Bert De Bièvre: 0000-0003-4203-5327
Wouter Buytaert: 0000-0001-6994-4454

Competing interests

The authors declare no competing interests.

Acknowledgements

Special thanks to the people of Huamantanga and their authorities for providing constant participation, support, and consent to our work. The paired catchment monitoring and the infiltration system restoration were set up thanks to funding from The Natural Capital Project, CONDESAN, Alternativa NGO, AQUAFONDO, and TNC. We thank SENAMHI, ANA, and iMHEA for the hydrometeorological data provided. We acknowledge funding from UK Research and

Innovation (NERC grant NE/K010239-1), and the Natural Infrastructure for Water Security Project funded by USAID and the Government of Canada. B.O.T. was funded by an Imperial College President's PhD Scholarship and the Science and Solutions for a Changing Planet DTP (UKRI NERC grant NE/L002515/1). W. Lavado and F. Vega-Jácome provided useful information for the interpretation of regional hydrometeorological data. A. Butler and C. Hackshaw provided helpful comments on the manuscript. Fig. 2 was developed with help from Soapbox Communications Ltd.

References

[1] Van Loon, A. F. et al. Drought in the Anthropocene. *Nat. Geosci.* **9**, 89–91 (2016).
[2] Mishra, A. K. & Singh, V. P. A review of drought concepts. *J. Hydrol.* **391**, 202–216 (2010).
[3] Van Loon, A. F. Hydrological drought explained. *WIREs Water* **2**, 359–392 (2015).
[4] Ledger, M. E., Brown, L. E., Edwards, F. K., Milner, A. M. & Woodward, G. Drought alters the structure and functioning of complex food webs. *Nat. Clim. Change* **3**, 223–227 (2012).
[5] van Vliet, M. T. H. et al. Vulnerability of US and European electricity supply to climate change. *Nat. Clim. Change* **2**, 676–681 (2012).
[6] von Uexkull, N., Croicu, M., Fjelde, H. & Buhaug, H. Civil conflict sensitivity to growing-season drought. *Proc. Natl. Acad. Sci. USA* **113**, 12391–12396 (2016).
[7] UN-WATER. *The United Nations World Water Development Report 2018: Nature-Based Solutions for Water* (UNESCO: Paris, France, 2018).
[8] Ministry of Environment of Peru. *Ley No. 30215 De Mecanismos De Retribución Por Servicios Ecosistémicos – Law No. 30215 on Reward Mechanisms for Ecosystem Services* (El Peruano: Lima, Peru, 2014).
[9] Somers, L. D. et al. Does hillslope trenching enhance groundwater recharge and baseflow in the Peruvian Andes? *Hydrol. Process.* **32**, 318–331 (2018).
[10] Grainger, S. et al. The development and intersection of highland-coastal scale frames: a case study of water governance in central Peru. J. Environ. Pol. Plan. https://doi.org/10.1080/1523908X.2019.1566057 (2019).
[11] Ávila, J. *El Sistema de Infiltración Hídrica para el Mamanteo de Huamantanga – The Water Infiltration System for Huamantanga's Mamanteo* (Alternativa NGO: Huamantanga, Peru, 2012).
[12] Apaza, D., Arroyo, R., & Alcencastre, A. *Las Amunas de Huarochirí, Recarga de Acuíferos en los Andes – The Amunas of Huarochirí, Aquifer Recharge in the Andes* (Gestión Social del Agua y Ambiente en Cuencas – GSAAC: Lima, Peru, 2006).
[13] Garnett, S. T. et al. A spatial overview of the global importance of Indigenous lands for conservation. *Nat. Sustain.* **1**, 369–374 (2018).
[14] Beckers, B., Berking, J. & Schutt, B. Ancient Water Harvesting Methods in the Drylands of the Mediterranean and Western Asia. *J. Anc. Stud.* **2**, 145–164 (2008).
[15] Dande, R., Bele, A., Padgilwar, P.P. & Kulkarni, N. Sustainable rain water harvesting techniques prevailing in ancient India. *Int. J. Theor. Appl. Res. Mech. Eng.* **5**, 16–24 (2016).
[16] DiNapoli, R. J. et al. Rapa Nui (Eastern Island) monument (ahu) locations explained by freshwater sources. *PLoS ONE* **14**, e0210409 (2019).
[17] Brosnan, T., Becker, M.W. & Lipo, C.P. Coastal groundwater discharge and the ancient inhabitants of Rapa Nui (Easter Island), Chile. *Hydrogeol. J.* **27**, 519–534 (2019).
[18] Pulido-Bosch, A. & Ben Sbih, Y. Centuries of artificial recharge on the southern edge of the Sierra Nevada (Granada, Spain). *Environ. Geol.* **26**, 57–63 (1995).
[19] Headworth, H. G. Early Arab water technology in Southern Spain. *Water Environ. J.* **18**, 161–165 (2004).

[20]Wright, K. R., & Valencia Zegarra, A. *Machu Picchu: A Civil Engineering Marvel* (ASCE Press: Reston, VA, USA, 2000).
[21]Wright, K. R., Witt, G. D., Valencia Zegarra, A. Hydrogeology and paleohydrology of ancient Machu Picchu. *Groundwater* **35**, 660–666 (1997).
[22]Vogl, A. L. et al. (2017) Mainstreaming investments in watershed services to enhance water security: Barriers and opportunities. *Environ. Sci. Policy* **75**, 19–27 (2017).
[23]Manz, B. et al. High-resolution satellite-gauge merged precipitation climatologies of the Tropical Andes. *J. Geophys. Res. Atmos.* **121**, 1190–1207 (2016).
[24]Boers, N., Bookhagen, B., Marwan, N., Kurths, J. & Marengo, J. Complex networks identify spatial patterns of extreme rainfall events of the South American Monsoon System. *Geophys. Res. Lett.* **40**, 4386–4392 (2013).
[25]Romatschke, U. & Houze, R. A. Extreme summer convection in South America. *J. Climate* **23**, 3761–3791 (2010).
[26]Garreaud, R. D. The Andes climate and weather. *Adv. Geosci.* **22**, 3–11 (2009).
[27]Houston, J. & Hartley, A. The central Andean west-slope rainshadow and its potential contribution to the origin of hyperaridity in the Atacama Desert. *Int. J. Climatol.* **23**, 1453–1464 (2003).
[28]Chen, D., Cane, M. A., Kaplan, A., Zebiak, S. E. & Huang, D. Predictability of El Niño over the Past 148 Years. *Nature* **428**, 733–736 (2004).
[29]De Bièvre, B. & Acosta, L. in *Mountains and Climate Change: A Global Concern* (eds Kohler, T., Wehrli, A. & Jurek, M.) *Andean Water for Peru's Coastal Deserts*, 32–34 (Centre for Development and Environment (CDE), Swiss Agency for Development and Cooperation (SDC), and Geographica Bernensia: Bern, Switzerland, 2014).
[30]Ochoa-Tocachi, B. F., Buytaert, W. & De Bièvre, B. Regionalization of land-use impacts on streamflow using a network of paired catchments. *Water Resour. Res.* **52**, 6710–6729 (2016).
[31]Bonnesoeur, V. et al. Impacts of forests and forestation on hydrological services in the Andes: A systematic review. *For. Ecol. Manag.* **433**, 569–584 (2019).
[32]Bradley, R. S., Vuille, M., Diaz, H. F. & Vergara, W. Climate change. Threats to water supplies in the tropical Andes. *Science* **312**, 1755–1756 (2006).
[33]Buytaert, W., Célleri, R. & Timbe, L. Predicting climate change impacts on water resources in the tropical Andes: Effects of GCM uncertainty. *Geophys. Res. Lett.* **36**, L07406 (2009)
[34]Viviroli, D. et al. Climate change and mountain water resources: Overview and recommendations for research, management and policy. *Hydrol. Earth Syst. Sci.* **15**, 471–504 (2011).
[35]Ragettli, S., Immerzeel, W. W. & Pellicciotti, F. Contrasting climate change impact on river flows from high-altitude catchments in the Himalayan and Andes Mountains. *Proc. Natl. Acad. Sci. USA* **113**, 9222–9227 (2016).
[36]Gammie, G. & De Bièvre, B. *Assessing Green Interventions for the Water Supply of Lima, Peru* (Forest Trends: Washington DC, USA, 2015).
[37]Vega-Jácome, F., Lavado-Casimiro, W. & Felipe-Obando, O. Assessing hydrological changes in a regulated river system over the last 90 years in Rimac Basin (Peru). *Theor. Appl. Climatol.* **132**, 347–362 (2018).
[38]Gutiérrez, O. F. *Huamantanga: Tierra Fecunda, Heroica y Legendaria – Huamantanga: Fertile, Heroic, and Legendary Land* (Orlando Francisco Gutiérrez Reymundo: Lima, Peru, 2018).
[39]Ministry of Agriculture of Peru. *Rumbo a un Programa Nacional de Siembra y Cosecha de Agua: Aportes y Reflexiones Desde la Práctica - Towards a National Programme of Water Harvesting: Contributions and Insights From the Practice* (Ministerio de Agricultura y Riego del Perú, Viceministerio de Políticas Agrarias: Lima, Peru, 2016).

[40] Ochoa-Tocachi, B. F. et al. Impacts of land use on the hydrological response of tropical Andean catchments. *Hydrol. Process.* **30**, 4074–4089 (2016).

[41] Zulkafli, Z. et al. User-driven design of decision support systems for polycentric environmental resources management. *Environ. Model. Softw.* **88**, 58–73 (2017).

[42] Vitvar, T., Aggarwal, P. K. & McDonnell, J. J. in *Isotopes in the Water Cycle: Past, Present and Future of a Developing Science* (eds Aggarwal, P. K., Gat, J. R., & Froehlich, K.F.) *A Review of Isotope Applications in Catchment Hydrology*, 151–169 (Springer: Dordrecht, Netherlands, 2005).

[43] Jasechko, S., Kirchner, J. W., Welker, J. M. & McDonnell, J. J. Substantial proportion of global streamflow less than three months old. *Nat. Geosci.* **9**, 126–129 (2016).

[44] Gleick, P. H. & Palaniappan, M. Peak water limits to freshwater withdrawal and use. *Proc. Natl. Acad. Sci. USA* **107**, 11155–11162 (2010).

[45] Hommes, L. & Boelens R. From natural flow to 'working river': Hydropower development, modernity and socio-territorial transformations in Lima's Rímac Watershed. *J. Hist. Geogr.* **62**, 85–95 (2018).

[46] Welch, L. A., & Allen, D. M. Consistency of groundwater flow patterns in mountainous topography: Implications for valley bottom water replenishment and for defining groundwater flow boundaries. *Water Resour. Res.* **48**, W05526 (2012).

[47] Hall, J. S., Kirn, V. & Yanguas-Fernández, E. *Managing Watersheds for Ecosystem Services in the Steepland Neotropics* (Smithsonian Tropical Research Institute: Panama City, Panama, 2015).

[48] Ministry of Housing, Construction, and Sanitation of Peru. *Ley No. 30045 De Modernización De Los Servicios De Saneamiento – Law No. 30045 on Modernisation of Sanitation Services* (El Peruano: Lima, Peru, 2013).

[49] Kaser, G., Grosshauser, M. & Marzeion, B. Contribution potential of glaciers to water availability in different climate regimes. *Proc. Natl. Acad. Sci. USA* **107**, 20223–20227 (2010).

[50] Buytaert, W. et al. Glacial melt content of water use in the tropical Andes. *Environ. Res. Lett.* **12**, 114014 (2017).

[51] Tovar, C., Arnillas, C. A., Cuesta, F. & Buytaert, W. Diverging Responses of Tropical Andean Biomes under Future Climate Conditions. *PLoS ONE* **8**, e63634 (2013).

[52] Buytaert, W. & De Bièvre, B. Water for cities: The impact of climate change and demographic growth in the tropical Andes. *Water Resour. Res.* **48**, W08503 (2012).

[53] Romero-López, M. & Collado-Solís, C. *Acercamiento a las Estrategias de Vida de las Familias Rurales de Matiguás y Río Blanco – Approach to the Life Strategies of the Rural Families of Matiguás and Río Blanco* (Instituto de Investigación y Desarrollo: Managua, Nicaragua, 2013).

[54] Bastiaensen, J., Merlet, P. & Flores, S. *Rutas de Desarrollo en Territorios Humanos: Las Dinámicas de la Vía Láctea en Nicaragua – Development Pathways in Human Territories: Dynamics of the Milky Way in Nicaragua* (UCA Publicaciones: Managua, Nicaragua, 2015).

[55] Buytaert, W. et al. Citizen science in hydrology and water resources: opportunities for knowledge generation, ecosystem service management, and sustainable development. *Front. Earth Sci.* **2**, 1-21 (2014).

[56] Aley, T. *Groundwater Tracing Handbook* (Ozark Underground Laboratory: Protem, MO, USA, 2002).

[57] Ochoa-Tocachi, B. F. et al. High-resolution hydrometeorological data from a network of headwater catchments in the tropical Andes. *Sci. Data* **5**, 180080 (2018).

[58] Gustard, A., Bullock, A. & Dixon, J. M. *Low flow estimation in the United Kingdom. Report No. 108* (Institute of Hydrology: Wallingford, United Kingdom, 1992).

[59]Hollister, V.F. & Sirvas, E.B. The Calipuy Formation of Northern Peru, and its relation to volcanism in the Northern Andes. *J. Volcanol. Geotherm. Res.* **4**, 89–98 (1978).

[60]Lerner, D. N., Mansell-Moullin, M., Dellow, D. J. & Lloyd, J. W. Groundwater studies for Lima, Peru. *IAHS Publ.* **135**, 17–30 (1982).

[61]Geological, Mining, and Metallurgical Institute of Peru. *Hydrogeological Map of Peru* (Instituto Geológico, Minero y Metalúrgico del Perú: Lima, Peru, 2016).

[62]Kieser, M. S. *Restoration of Amunas: Quantifying Potential Baseflow Improvements* (Forest Trends: Lima, Peru, 2014).

[63]U.S. Geological Survey. *Shuttle Radar Topography Mission (SRTM) 1 Arc-Second Global: SRTM1S13W077V3* (U.S. Geological Survey (USGS) Earth Resources Observation and Science (EROS) Center: Sioux Falls, SD, USA, 2014)

[64]Van Loon, A. F., Laaha, G. Hydrological drought severity explained by climate and catchment characteristics. *J. Hydrol.* **526**, 3–14 (2015).

[65]Beyene, B. S., Van Loon, A. F., Van Lanen, H. A. J. & Torfs, P. J. J. F. Investigation of variable threshold level approaches for hydrological drought identification. *Hydrol. Earth Syst. Sci. Discuss.* **11**, 12765–12797 (2014).

[66]Ochoa-Tocachi, B. F. Computer code for data processing and simulation of pre-Inca infiltration enhancement systems (mamanteo and amunas). *GitHub* https://github.com/topicster/mamanteo (2019).

[67]Rosero-López, D. et al. Streamlined eco-engineering approach helps define environmental flows for tropical Andean headwaters. Freshw. Biol. https://doi.org/10.1111/fwb.13307 (2019).

Article accepted for publication in the journal Nature Sustainability
https://doi.org/10.1038/s41893-019-0307-1

Supplementary Information

Title
Potential contributions of pre-Inca infiltration infrastructure to Andean water security

Authors
Boris F. Ochoa-Tocachi, Juan D. Bardales, Javier Antiporta, Katya Pérez, Luis Acosta, Feng Mao, Zed Zulkafli, Junior Gil-Ríos, Oscar Angulo, Sam Grainger, Gena Gammie, Bert De Bièvre, and Wouter Buytaert

*corresponding author(s): Boris F. Ochoa-Tocachi (boris.ochoa13@imperial.ac.uk)

This file includes:

Supplementary Discussion
Supplementary Figs. 1 to 7
Supplementary Tables 1 to 9

Other supplementary materials for this manuscript include the following:

Supplementary Data 1. Ochoa-Tocachi, B. F. et al. High-resolution hydrometeorological data from a network of headwater catchments in the tropical Andes. *Figshare* https://doi.org/10.6084/m9.figshare.c.3943774 (2018).

Supplementary Data 2. National Service of Meteorology and Hydrology of Peru (SENAMHI). Time series of precipitation at Chosica and Huamantanga stations. *GitHub* https://github.com/topicster/mamanteo (2019).

Supplementary Data 3. National Water Authority (ANA). Time series of river flow in the Rimac river at the Chosica station. *GitHub* https://github.com/topicster/mamanteo (2019).

Supplementary Discussion

On the relation between water scarcity, drought and hydrological regulation. Human activities modify several components of the hydrological cycle, by altering fluxes such as evapotranspiration or soil infiltration, and by changing the water storage and response characteristics of catchments. Drought is different from low flows, water scarcity, and aridity in its temporal characteristics[3]. Droughts are episodic events of exceptional lack of water in the hydrological system compared to normal conditions[1]. Low flows are recurrent rather than exceptional minima, often on an annual basis. Water scarcity, in contrast, reflects long-term imbalances between water supply and water demand[3]. Similarly, aridity is a permanent feature of low precipitation climates[2]. Along the Pacific coast of Peru, these features combine and reinforce each other: droughts occurring during low flow (dry) season in an arid climate that suffers from water scarcity. Supplementary Fig. 1 illustrates precipitation seasonality and water deficit in the Rimac river basin and the consequences for Lima's water supply. Because of the high seasonality of precipitation in the highlands (Supplementary Fig. 1a) and arid nature of the lowlands (Supplementary Fig. 1b), low flows, droughts, and water scarcity conditions are common and occur simultaneously.

Terrestrial ecosystems provide a hydrological buffer to the variability of precipitation as water travels through a catchment, which is often referred to as a catchment's hydrological regulation capacity[30,31,40], and provides river flow during dry periods. Water supply systems that draw from surface water resources are very dependent on natural hydrological regulation to stabilise the intensity and timing of river flows. This is particularly challenging for Lima, which experiences a deficit of approximately 43 million m^3 of water during the dry season[36]. The surplus water during the wet season (December to May) is sufficient to meet the city's water demand during the dry season (June to November) but needs to be stored (Supplementary Fig. 1c). Water also needs to be stored on an interannual time scale to buffer severe and sustained droughts, such as those occurred in 1989–1992 (Supplementary Fig. 1d), and to reduce peak flows that can generate floods, such as the highest rainfall volumes observed in during the 1997–98 El Niño event, the most powerful in recorded history.

Lima relies on surface water for around 70% of its water supply. This is provided by three river basins (Rimac, Chillon, and Lurin) that drain to the Pacific, and complemented with water transfers from the Mantaro basin, which drains to the Atlantic (Supplementary Fig. 2)[45]. The community of Huamantanga is located in the Chillon river basin at an elevation of 3300 m a.s.l. The pre-Inca infiltration enhancement system in Huamantanga is located between 3500 and 4000 m a.s.l. and is used to delay wet season flow from the highlands to make it available during the dry season for the community. Products from the participatory mapping with local community members are shown in Supplementary Fig. 3. Analogies between the 'careo' system in Spain[18] and the 'mamanteo' system in Peru are shown in Supplementary Table 1. Similar methods have recently come to the attention of policy makers at national and international level as part of a portfolio of 'nature-based solutions' to improve water security and contribute to climate change adaptation for cities[7,8,10,11,12,22,34,36,38,39,48,62].

Implementation of the basin-scale hydrological model. The computational model to simulate the potential impact of upscaling infiltration systems on the river flow regime consists of the following steps:

1. Estimate the contribution area A_C to the infiltration systems from the total area of the river basin A_R.
2. Estimate the average precipitation over these areas, P_C and P_R, respectively.
3. Determine rainfall volumes for the periods when the infiltration systems are in operation, $P_{C,OP}$ and $P_{R,OP}$, respectively, (e.g., during the wet season).

4. Estimate the discharge volumes over this period $Q_{C,OP}$ and $Q_{R,OP}$, respectively, (e.g., using an average runoff ratio (RR) or water balance):
$$Q = RR \cdot P$$
5. Estimate the potential diversion ratio r_{div} to the infiltration systems using the calculated discharge volumes and the geometric and hydraulic characteristics of the diversion canals. These characteristics can be summarised in a coefficient c_{div} for long time scales (e.g. annual):
$$r_{div} = c_{div} \frac{Q_{C,OP}}{Q_{R,OP}}$$
6. Applying this factor to the time series of basin flow q(t), generates time series of diverted flow $q_{inf}(t)$ during the operation of the system:
$$q_{inf}(t) = \begin{cases} r_{div} \cdot q(t) & operation \\ 0 & otherwise \end{cases}$$
7. Calculate the time series of remaining flows $q_{rem}(t)$ in the river, which is the part of the discharge that is not diverted:
$$q_{rem}(t) = q(t) - q_{inf}(t)$$
8. Generate the new time series of modified river flows $q_{mod}(t)$ using the residence time distribution function of the infiltration system as a unit hydrograph –UH(t) from t_1 to t_2– to convolute the infiltrated water flow $q_{inf}(t)$ and applying the estimated recovery rate c_{rr}.
$$q_{mod}(t) = q_{rem}(t) + c_{rr} \cdot q_{inf}(t) * UH(t)$$

Supplementary Fig. 4 shows the steps involved in calculating the residence times and to use them to derive a unit hydrograph to replicate the effects of the infiltration system. The baseflow of the catchment upstream to the infiltration area was used to estimate spring discharge (Supplementary Fig. 4a). The tracer concentration from the experiments is used as a proxy for tracer concentration in the springs, which in turn is an indication of the relative contribution of infiltrated water to spring discharge (Supplementary Fig. 4b). The subsurface unit hydrograph of the infiltration water was then obtained by interpolating the tracer concentration data at daily temporal resolution, scaling them by the baseflow, and normalising them to sum 1 (Supplementary Figs. 4c and 4d). The result of the simulation of the infiltration practice compared to the original hydrograph is shown in Supplementary Fig. 4e. Potential effects of replicating the infiltration system are illustrated at monthly temporal resolution at, respectively, local scale for the community of Huamantanga using catchments C1 and C2 (Supplementary Fig. 5), and at regional scale for Rimac's river flow (Supplementary Figs. 6–8). Supplementary Table 2 shows the measured eosin tracer concentrations in the four studied springs. The dye tracers were injected in the diversion canals on March 21, 2015 and collected using activated carbon samplers at irregular intervals. Average cumulative and daily concentrations are shown in Supplementary Table 3.

Supplementary Tables 4 and 5 show average monthly precipitation and discharge for the area of the Rimac river basin above 4,000 m a.s.l. (1,428.1 km^2), and for the contributing area to the Chosica station (2,318.8 km^2), respectively (Supplementary Fig. 2). The total Rimac river basin area discharging at sea level is 3,503.9 km^2. Mean monthly precipitation climatologies for 1998 to 2014 were obtained by merging TRMM satellite data with rain gauge data using a residual ordinary Kriging (ROK) technique[23] (Supplementary Fig. 6). Monthly discharge was calculated by applying a runoff ratio to the precipitation data, which was estimated as the average runoff ratio of the monitored catchments C1 and C2 (22.44%)[57]. We cross-validated the TRMM-based precipitation estimates for the highlands with our rainfall records in Huamantanga and found a good match (annual TRMM-based climatology of 505

mm yr^{-1} compared to the rain-gauge amount of 545 mm yr^{-1}), despite the different time period. In contrast, Rimac's discharge data measured at the Chosica station seem to be overestimated (annual TRMM-based climatology of 437 mm yr^{-1} compared to discharge volume at the Chosica station of 419 mm yr^{-1} would result in a runoff ratio of 96% that cannot be simply explained by water transfers from the Mantaro basin).

Supplementary Tables 6 and 7 show the meteorological and hydrological drought characteristics of the Rimac basin. The headwaters of Lima experience a monomodal precipitation pattern, with high drought risk typically caused by either a delayed start of the rains, and early end of the rains, or anomalously low rainfall volumes. Historically, fewer than one drought event occurs per year on average, which suggests that those three conditions rarely happen simultaneously. Results from a most recent period of analysis (1990–2018) against the longer historic records (1964–2018) reveal that drought events have become more frequent (1.38 yr^{-1} vs 0.74 yr^{-1}), they last for longer (maximum durations of 167 days vs 123 days), and maximum water deficits have become more pronounced (79.9 mm vs 73.0 mm). Rainfall in the city of Lima is negligible, and although drought events are technically less frequent (0.53 yr^{-1}) and can span for up to 68 days, resulting water deficit volumes during drought account for a maximum of 2 mm (Supplementary Table 6). Hydrological drought characteristics indicate that artificial hydrological regulation (grey infrastructure) have reduced the occurrence and negative impacts of droughts (Supplementary Table 7). Under this analysis, our simulated flow diversions in the upscaled infiltration systems have only a limited effect on the magnitude and extent of droughts.

Supplementary Table 8 shows a sensitivity analysis of the recovery rate to estimate regional effects of upscaling the infiltration systems to the source areas of Lima. The estimated recovery rate of 0.5 is based on a calculation of losses from evapotranspiration and deep percolation. At regional scale, the recovery rate could differ because of natural geographical and climatic characteristics[46]. It might be expected that losses due to percolation at local scale return to the hydrological network further downstream and so, a larger recovery rate can be expected for the Rimac river basin (0.6 or up to 0.7). However, we also present the results obtained with a recovery rate of 0.4 to put the results in context. The results of the sensitivity analysis are also shown in Supplementary Fig. 7. Supplementary Fig. 8 shows the regional effects of upscaling the infiltration systems but assuming that water diversion occurs from January to April (discarding diversion in December) to reduce the impacts of a delay in the start of the rains in the wet season. This corresponds to a recovered volume of which results in 87 $x10^6 m^3 yr^{-1}$ in contrast to the 99 $x10^6 m^3 yr^{-1}$ when including December diversions.

Extended data. Supplementary Table 9 shows details of the meetings and participants of the social science research conducted to access the local knowledge about the ancient infiltration practices and to record their field experiences in relation to the operation and maintenance of the infiltration system.

The hydrological monitoring data is described in a Data Descriptor[57], the custom code used for this study is available in a public repository[66], and supplementary data are available in Supplementary Data 1–3.

Article accepted for publication in the journal Nature Sustainability
https://doi.org/10.1038/s41893-019-0307-1

Supplementary Figures

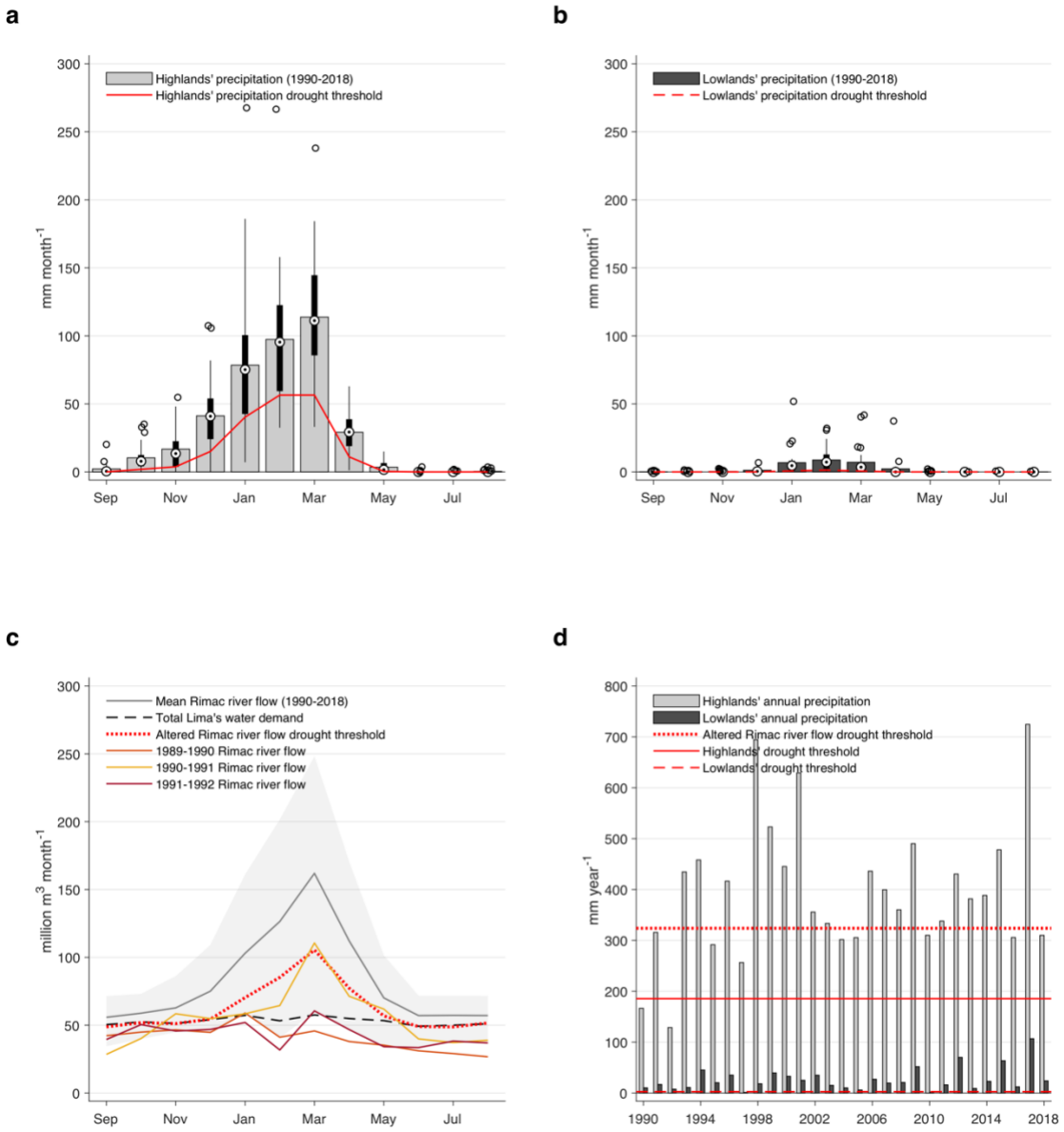

Supplementary Fig. 1 | Precipitation variability and water deficit in Lima, Peru. **a**, Monthly precipitation in the Huamantanga station (11°30'0.0"S, 76°45'0.0"W, 3392m a.s.l.) from 1990 to 2018; **b**, Monthly precipitation at the Chosica station (11°55'47.5"S, 76°41'22.8"W, 863 m a.s.l.) near Lima from 1990 to 2018. For a and b, bars represent the mean, target symbols show the median, black boxes are limited by the 25th and 75th percentiles in monthly precipitation, whiskers correspond to ±2.7σ and extends to the adjacent data value that is not an outlier, and outliers are shown as white circles. **c**, Average monthly water supply and demand in the Rimac River basin (Chosica station), drought threshold, and selected severely dry years. Variability is represented by the shaded areas using 5th and 95th percentiles of monthly data. Red lines in all plots represent drought conditions using a variable threshold level approach[64,65], based on a 30-day moving average method and defined at the 20th percentile of inter-annual data from 1990 to 2018. **d**, Time series of annual precipitation in both stations from 1990 to 2018 and accumulated annual drought thresholds. The drought threshold for the Chosica station in the lowlands is very close to zero (see also Supplementary Tables 6 and 7).

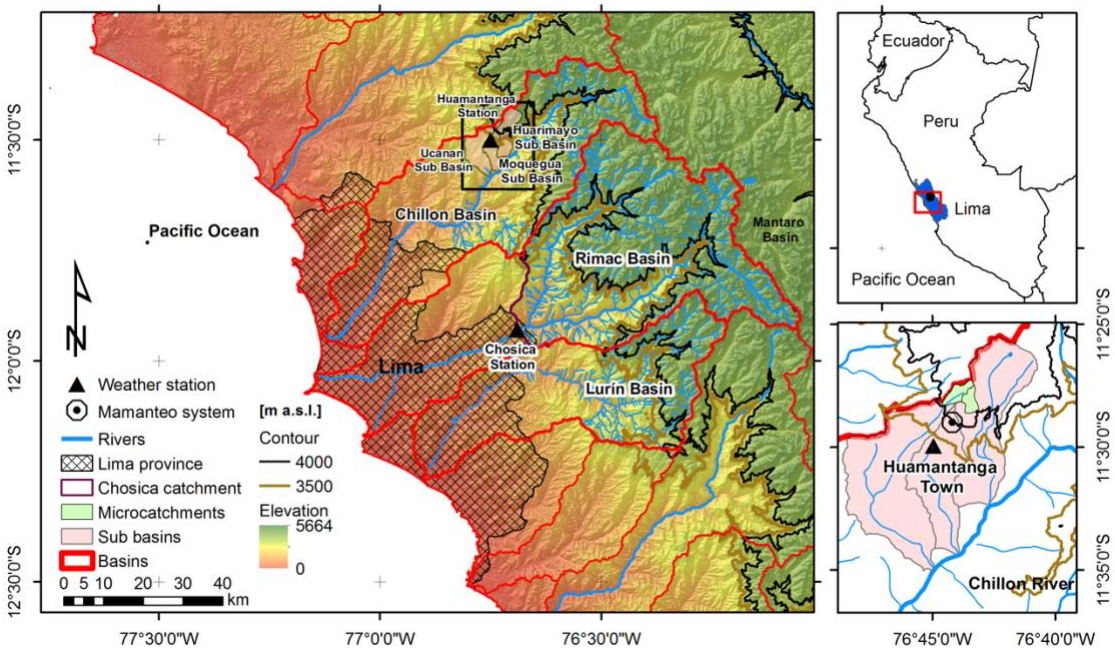

Supplementary Fig. 2 | Location of the community of Huamantanga, the city of Lima, and the main basins that supply water to Lima. Black triangles illustrate the location of the weather stations whose data is shown in Fig. 1 and Supplementary Fig. 1 (Chosica and Huamantanga). The four main basins that supply water to Lima (Chillon, Rimac, Lurin, and Mantaro) are delineated in bold red. The two monitored microcatchments C1 and C2 and the location of the infiltration system in Huamantanga are shown in the subplot (bottom right). Two reference elevation values (4000 and 3500 m a.s.l.) used for the calculation of potential scalability of the infiltration system are depicted in the map as black and brown lines, respectively.

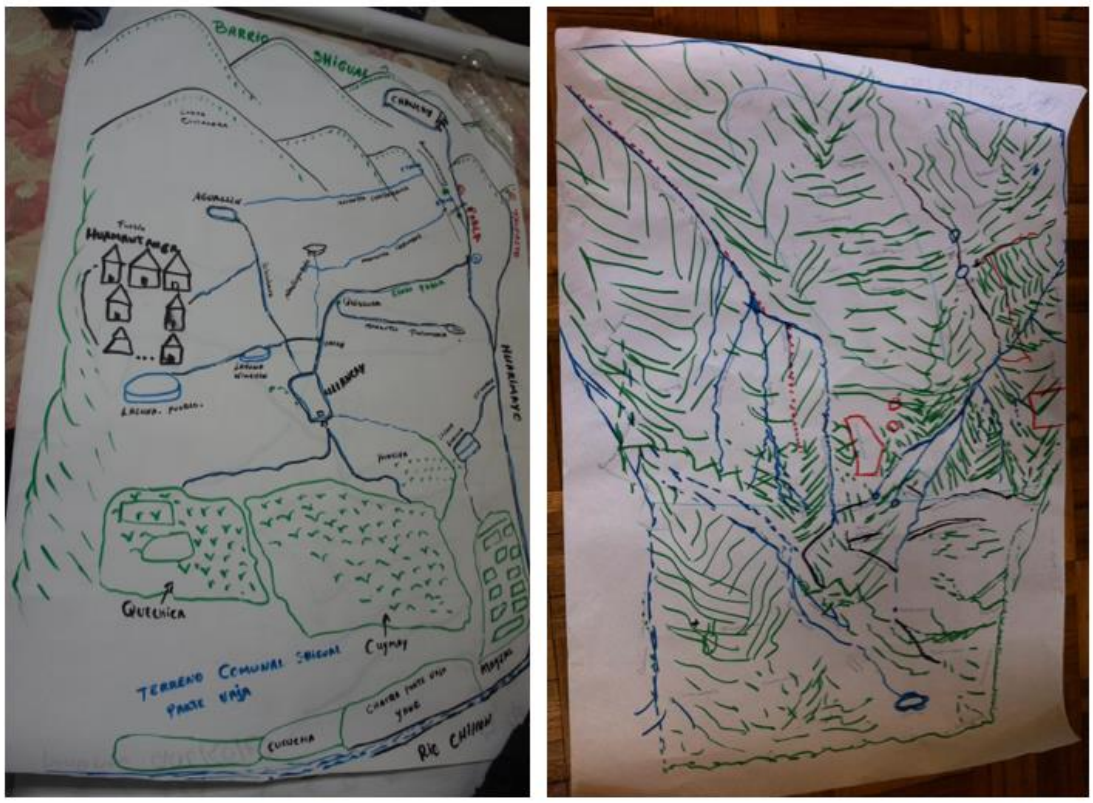

Supplementary Fig. 3 | Products of the participatory mapping with local community members. The photographs show posters generated in meetings with the two neighbourhoods in the community of Huamantanga to identify the elements that constitute the infiltration system and the livelihoods supported by water use. These products were subsequently used to map the system in the field and were digitised to create Fig. 3 as shown in the main text.

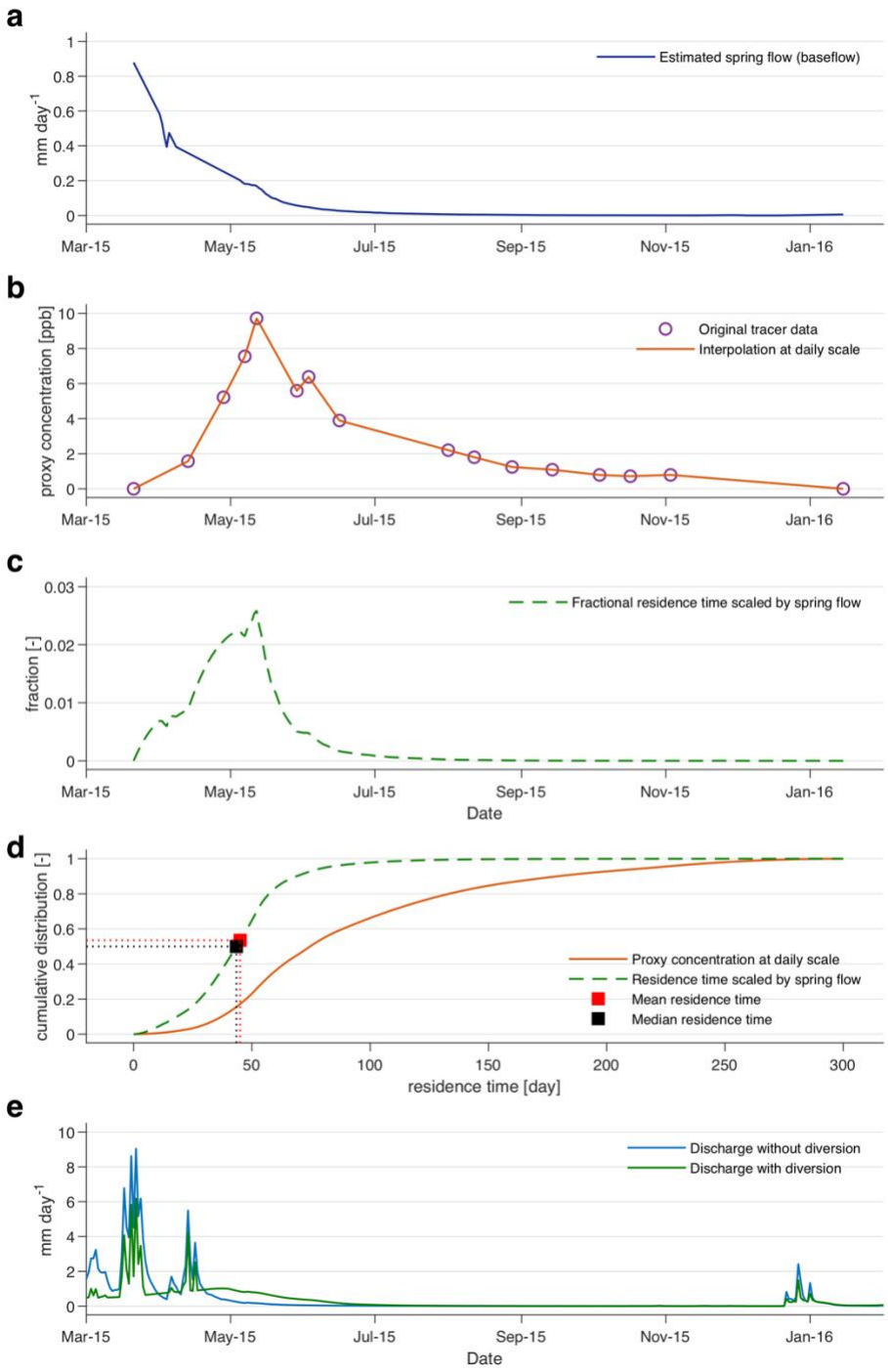

Supplementary Fig. 4 | Calculation of residence times to estimate flow resurface downstream. a, Spring flow during the analysed time window is approximated from baseflow in the monitored catchment C1. **b**, Measured tracer concentrations (Supplementary Table 3) and data interpolated at daily scale. **c**, Daily residence time distribution obtained from interpolating the tracer concentration, scaled by the estimated spring flow, and normalised to sum 1. **d**, Cumulative residence time distributions showing tracer concentration interpolated at daily scale and residence time scaled by baseflow; mean and median values are illustrated as coloured squares. **e**, Example of original and modified hydrographs for the analysed time window illustrating the effects of flow diversion to the infiltration system and posterior downstream resurface. Diverted flows and resurface are calculated using the high-resolution 5-min streamflow data, residence times are scaled by the correspondent baseflows at each time step, recovery rate is estimated in 0.5, and modified flows are subsequently accumulated at daily scale.

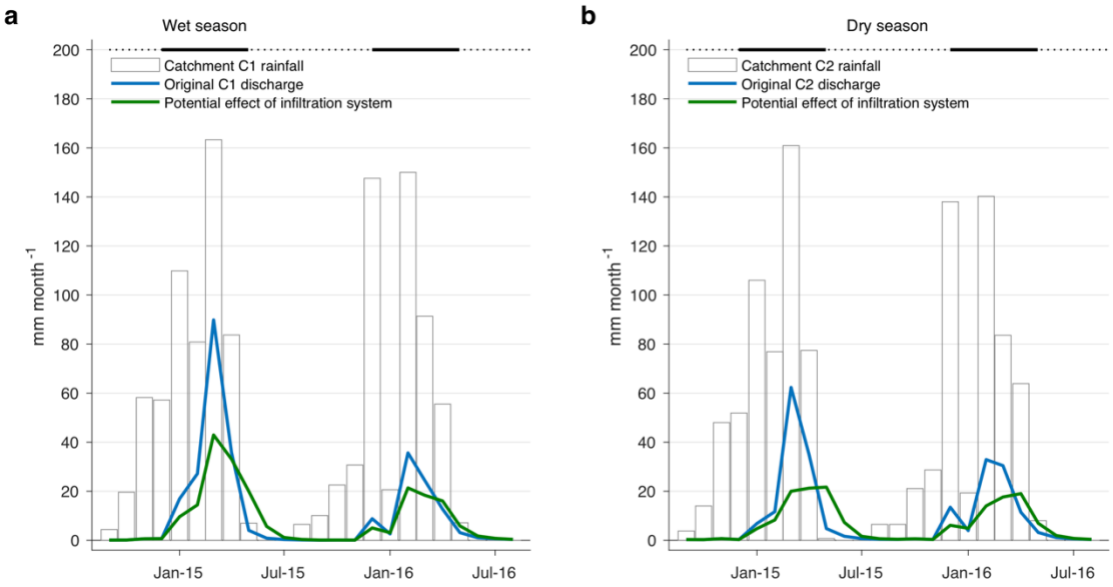

Supplementary Fig. 5 | Potential local effects of pre-Inca infiltration enhancement systems at monthly scale. Time series of rainfall, original discharge, and modified hydrographs are illustrated for catchments C1, **a**, and C2, **b**, respectively. Diverted flows and resurface are calculated using the high-resolution 5-min streamflow data, residence times are calculated from tracer concentrations scaled by the estimated spring flow, recovery rate is estimated in 0.5, and modified flows are subsequently accumulated at monthly scale.

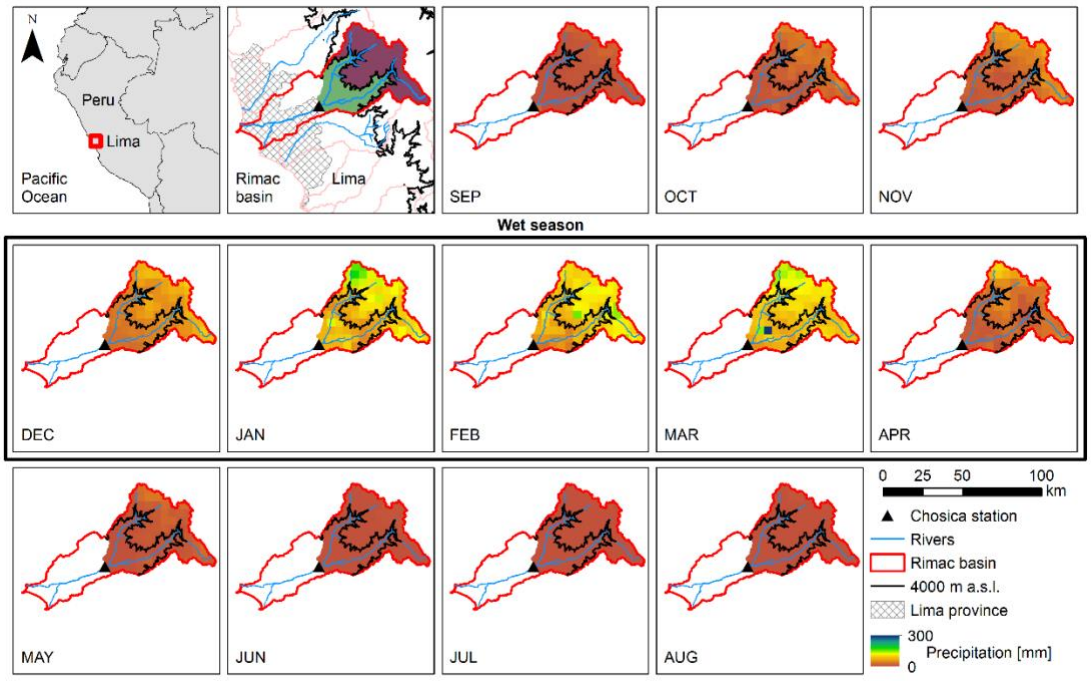

Supplementary Fig. 6 | Monthly rainfall climatologies for the Rimac river basin. Mean monthly precipitation climatologies for 1998 to 2014 obtained by merging TRMM satellite data with rain gauge data using a residual ordinary Kriging (ROK) technique[23].

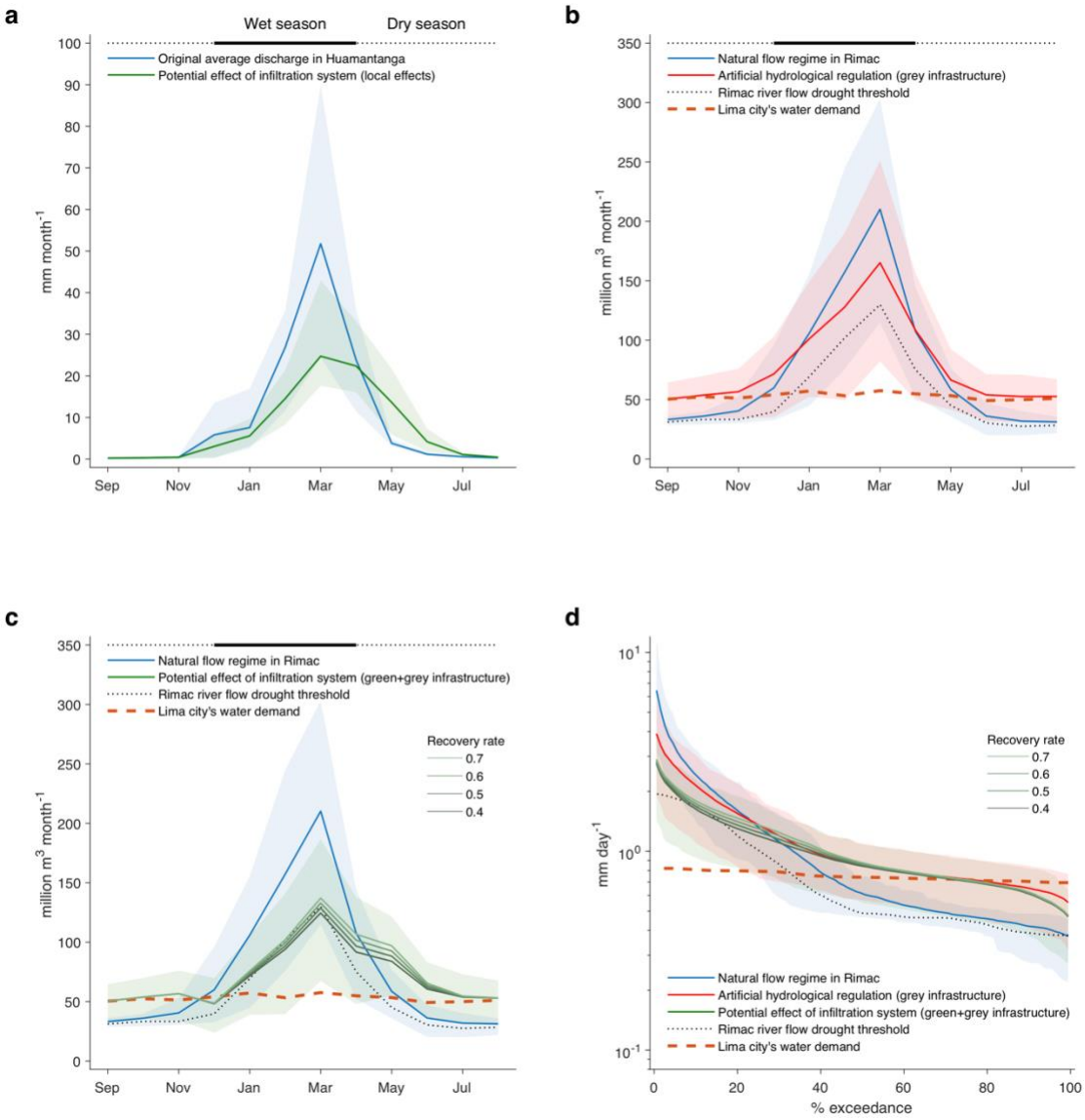

Supplementary Fig. 7 | Potential regional effects of pre-Inca infiltration enhancement systems at monthly scale. a, Local effects calculated as the monthly average from Huamantanga's data in catchments C1 and C2; **b**, Natural flow regime (1921–1960) vs the effect of artificial hydrological regulation, represented by the period when grey infrastructure projects have been implemented (1960–2018)[37]; **c**, Natural flow regime vs the potential effect of the infiltration system on top of that of the grey infrastructure; **d**, Mean annual flow duration curves of the natural flow regime (blue), artificial hydrological regulation (red), and potential effect of the infiltration system (green). Variability is represented by the shaded areas using 5th and 95th percentiles of monthly data. Black dotted lines represent natural hydrological drought conditions using a variable threshold level approach[64,65], based on a 30-day moving average method and defined at the 20th percentile of inter-annual data from 1921 to 1960. Diverted flows and resurface are calculated using the high-resolution 5-min streamflow data for Huamantanga and 1-day river flow data for Rimac, residence times are calculated from tracer concentrations scaled by the estimated spring flow, recovery rate is estimated in 0.5 locally and between 0.4–0.7 regionally, and modified flows are subsequently accumulated at monthly scale.

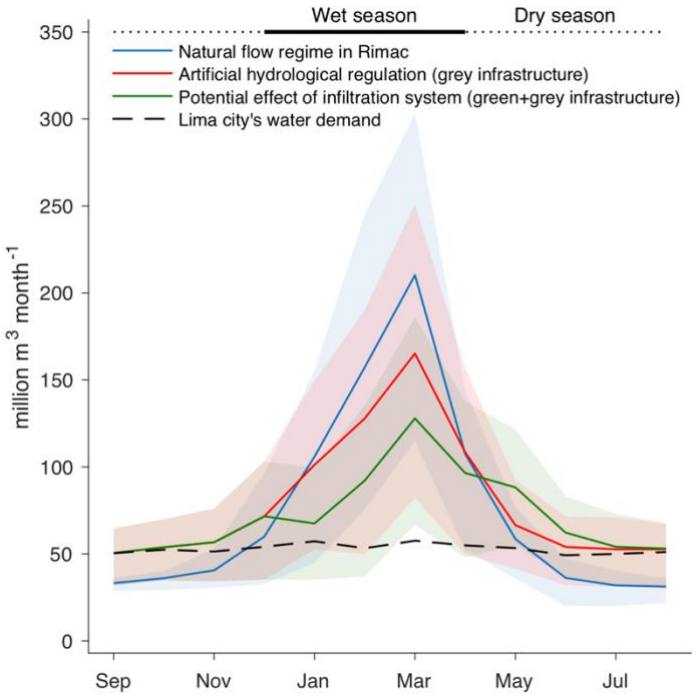

Supplementary Fig. 8 | Potential regional effects of pre-Inca infiltration enhancement systems with adjusted water diversion. The natural flow regime of the Rimac river (blue) is estimated from records covering the period 1921–1960. From 1960, the effect of grey infrastructure is evidenced by its artificial hydrological regulation effects (red), reducing wet season surplus and increasing dry season flows[37]. The potential effect of upscaling pre-Inca infiltration infrastructure (green) is estimated on top of that of the grey infrastructure. In contrast to Fig. 5, which considers water diversion to start with the rainy season on 01 of December, the calculation of water diversion here is assumed to occur from the 01 of January until the 30 of April each year. This reduces the impact of natural delays in the start of the rainy season and constitutes an example of how to fine-tune the operation of the systems, which could be also combined with an adjusted operation of the grey infrastructure. The recovery rate is estimated in 0.5, which results in 87 $x10^6 m^3 yr^{-1}$ that are recovered. Interannual variability is represented by the shaded areas using the 5^{th} and 95^{th} percentiles of monthly data. The dashed line represents Lima's total water demand[36].

Article accepted for publication in the journal Nature Sustainability
https://doi.org/10.1038/s41893-019-0307-1

Supplementary Tables

Supplementary Table 1 | Analogies between two ancient water harvesting practices: careo in Spain and mamanteo in Peru.

	Careo[18]	**Mamanteo**
Climate	Semiarid Rainfall 600–800 mm yr^{-1} Snowfall + snowmelt contribution to flow Evapotranspiration is 50% 23% of days are rainy days	Semiarid Rainfall 500–600 mm yr^{-1} No snowfall Evapotranspiration is 75% Rains five months a year
Elevation	Above 3000 m a.s.l.	Above 3500 m a.s.l.
Diversion channels	Known as '*acequias'*. Constructed during the 9th–15th century (by Arabs), and possibly older, 4th century (by the Romans) Unlined (lining was attempted but resulted in plant death along the irrigation channel as there is no soil moisture replenishment) Length several kilometres: the longest exceeds 15 km	Diversion and infiltration canals. Constructed by pre-Inca cultures, Chavín initially and Wari later, from as early as the 5th century Lined, followed by unlined Length usually short, the restored canal evaluated here is < 2 km
Recharge ponds	Directly accessible for irrigation Sediment cleared regularly	Directly accessible for irrigation Low sediment load and deposition
Outlets and residence time	Temporary springs ('remanentes', shallow flow, 5 days) Perennial springs ('fuentes', deeper subsurface flow, 10 days)	Downslope springs ('manantes', water is delayed from 2 weeks up to 8 months, with a mean of 45 days)
Yield	200 l s^{-1} recharge rates 10 l s^{-1} recovered in spring during recharge time 1 l s^{-1} recovered in spring during dry periods	75 l s^{-1} recharge rates Uncertain water yield and recovery rate
Management	Written rules governing usage and maintenance Scheduled irrigation	Community shared property Scheduled irrigation Cultural and religious practices around the system maintenance and operation
Agriculture	Rye, legume, vegetables; natural and planted trees and crops along the irrigation channels	Cattle pasture for cheese production, potato and corn cultivation mainly; mixed crops for self-consumption

Supplementary Table 2 | Eosin dye-tracer experiment results in downslope springs

Date [dd/mm/yyyy]		Interval [day]	Cumulative concentration [ppb day]			
Data placed	Data collected		Spring 1	Spring 2	Spring 3	Spring 4
21/03/2015	21/03/2015	0	0	0	0	0
21/03/2015	13/04/2015	23	6.1	57.3	66.9	14.5
13/04/2015	28/04/2015	15	4.8	115	143	50.1
28/04/2015	05/05/2015	7		75.2	102	
28/04/2015	07/05/2015	9	10			40.3
07/05/2015	12/05/2015	5	7.8	64.7	90.4	31.4
12/05/2015	29/05/2015	17	29.7	126	166	58.1
29/05/2015	03/06/2015	5	10.8	51.2	51.7	
29/05/2015	16/06/2015	18				50
03/06/2015	16/06/2015	13	12.6	64.1	89.6	
01/08/2015	12/08/2015	11	4.8		22.4	23.5
12/08/2015	28/08/2015	16	19.6	11	22.3	26.8
28/08/2015	14/09/2015	17	16.4		26.5	21.8
14/09/2015	04/10/2015	20	10	8.8	27.4	16.9
04/10/2015	17/10/2015	13	6.9	6.3	16.3	7.9
17/10/2015	03/11/2015	17	10.5	6.4	22.4	14.5

Supplementary Table 3 | Average eosin dye-tracer concentrations

Sampling date [dd/mm/yyyy]	Interval [day]	Average cumulative concentration [ppb day]	Average concentration [ppb]
21/03/2015	0	0	0
13/04/2015	23	36.19	1.57
28/04/2015	15	78.23	5.22
07/05/2015	9	67.94	7.55
12/05/2015	5	48.58	9.72
29/05/2015	17	94.95	5.59
03/06/2015	5	31.9	6.38
16/06/2015	13	50.6	3.89
01/08/2015	46	-	-
12/08/2015	11	19.78	1.80
28/08/2015	16	19.93	1.25
14/09/2015	17	18.51	1.09
04/10/2015	20	15.77	0.79
17/10/2015	13	9.33	0.72
03/11/2015	17	13.46	0.79

Supplementary Table 4 | Monthly precipitation and discharge estimated from the merged TRMM climatology[23] (1998–2014) over the portion of the Rimac river basin above 4000 m a.s.l.[a]

Month	Min [mm]	Max [mm]	Mean [mm]	Standard deviation [mm]	Discharge[b] [mm]	Volume [million m³]
Sep	0.29	36.74	9.02	5.49	2.02	2.89
Oct	3.51	53.24	27.71	10.86	6.22	8.88
Nov	5.22	85.91	37.77	16.48	8.48	12.11
Dec	**29.55**	**115.64**	**61.01**	**14.07**	**13.69**	**19.55**
Jan	**42.27**	**178.91**	**103.80**	**26.82**	**23.29**	**33.27**
Feb	**31.89**	**153.33**	**103.35**	**18.97**	**23.19**	**33.12**
Mar	**50.64**	**161.69**	**102.70**	**18.97**	**23.05**	**32.91**
Apr	**0.80**	**98.76**	**38.87**	**18.87**	**8.72**	**12.46**
May	0.79	52.00	14.70	8.41	3.30	4.71
Jun	0.16	7.49	2.22	1.98	0.50	0.71
Jul	0.01	7.17	0.96	1.26	0.21	0.31
Aug	0.17	7.86	2.81	1.69	0.63	0.90
Annual			504.92		113.31	161.82
Wet season[c]			409.73		91.95	131.31
Potential diversion					45.97	65.66

[a] Area of the Rimac river basin above 4000 m a.s.l. estimated from SRTM elevation data at 1-arc sec[62] is 1428.1 km^2.
[b] Assumed runoff ratio is 22.44%, estimated from iMHEA's Huamantanga data.
[c] Wet season ranges from December to April (in bold).
See also Supplementary Fig. 6.

Supplementary Table 5 | Monthly precipitation and discharge estimated from the merged TRMM climatology[23] (1998–2014) for the contributing area of the Rimac river basin to the Chosica station[a]

Month	Min [mm]	Max [mm]	Mean [mm]	Standard deviation [mm]	Discharge[b] [mm]	Volume [million m³]
Sep	0.28	36.74	6.96	5.63	1.56	3.62
Oct	3.51	53.24	21.51	12.31	4.83	11.19
Nov	2.05	85.91	29.98	16.96	6.73	15.60
Dec	**25.73**	**115.64**	**52.77**	**15.88**	**11.84**	**27.46**
Jan	**42.27**	**178.91**	**92.45**	**27.61**	**20.75**	**48.11**
Feb	**15.57**	**153.33**	**90.65**	**25.28**	**20.34**	**47.17**
Mar	**33.65**	**294.55**	**96.90**	**29.40**	**21.75**	**50.42**
Apr	**0.80**	**98.76**	**30.80**	**18.82**	**6.91**	**16.03**
May	0.59	52.00	10.84	8.60	2.43	5.64
Jun	0.12	7.49	1.82	1.83	0.41	0.94
Jul	0.01	7.17	0.76	1.07	0.17	0.39
Aug	0.17	7.86	2.01	1.75	0.45	1.04
Annual			437.44		98.17	227.63
Wet season[c]			363.57		81.59	189.19

[a] Contributing area of the Rimac river basin to the Chosica station estimated from SRTM elevation data at 1-arc sec[63] is 2318.8 km^2.
[b] Assumed runoff ratio is 22.44% as in the highlands. This is a conservative estimate given the larger evapotranspiration expected in the lowlands.
[c] Wet season ranges from December to April (in bold).
See also Supplementary Fig. 6.

Supplementary Table 6 | Meteorological drought characteristics in Huamantanga (3392 m a.s.l.) and Chosica (863 m a.s.l.) stations[a]

Station (period) [yr]	Mean ± std rainfall [mm yr^{-1}]	No. of droughts [yr^{-1}]	Mean ± std duration [day]	Max duration [day]	Mean ± std deficit [mm]	Max deficit [mm]
Huamantanga highlands (1964–2018)	354.6 ± 147.4	0.74	35.0 ± 27.7	123	-13.4 ± 16.1	-73.0
Huamantanga highlands (1990–2018)	380.3 ± 139.0	1.38	29.0 ± 30.3	167	-7.5 ± 15.3	-79.9
Chosica – Lima city (1990–2018)	25.9 ± 22.7	0.59	21.9 ± 16.3	68	-0.5 ± 0.6	-2.0

[a]See Fig. 1 and Supplementary Figs. 1a and 1b. Stations (**a**) Huamantanga, and (**b**) Chosica

Supplementary Table 7 | Hydrological drought characteristics in the Rimac river at the Chosica station[a]

Conditions (period) [yr]	Mean ± std streamflow [mm yr^{-1}]	No. of droughts [yr^{-1}]	Mean ± std duration [day]	Max duration [day]	Mean ± std deficit [mm]	Max deficit [mm]
Natural flow regime (1921–1960)	382.3 ± 88.6	1.25	53.0 ± 41.7	173	-5.7 ± 6.7	-22.1
Grey infrastructure (1961–2018)	407.5 ± 102.8	0.85	84.2 ± 92.8	422[b]	-11.9 ± 21.6	-104.5
Green+grey infrastructure (1961–2018)	365.6 ± 91.3	0.76	95.1 ± 96.1	419[b]	-12.3 ± 21.2	-96.6

[a] See Fig. 1 and Supplementary Fig. 1c. Station (**b**) Chosica
[b] The long drought duration refers to the extreme drought episodes during years 1989–1992 (see Supplementary Fig. 1d).

Supplementary Table 8 | Sensitivity analysis of the recovery rate to estimate regional effects of infiltration systems for the Rimac river basin

Recovery rate [-]	Recovered volume [$x10^6$ m^3 yr^{-1}]	Dry season flow increase [%]				
		Long-term monthly average	Long-term monthly max	Minimum monthly mean	Average monthly mean	Maximum monthly mean
0.40	79.1	6.03	56.86	0.02	5.99	26.52
0.50	**98.9**	**7.53**	**71.07**	**0.03**	**7.49**	**33.15**
0.60	118.6	8.94	85.29	0.03	8.99	39.79
0.70	138.4	10.48	99.50	0.04	10.49	46.42

Results for a recovery rate of 0.5 (in bold) are featured in the main text.

References in the Supplementary Material

[1] Van Loon, A. F. et al. Drought in the Anthropocene. *Nat. Geosci.* **9**, 89–91 (2016).

[2] Mishra, A. K. & Singh, V. P. A review of drought concepts. *J. Hydrol.* **391**, 202–216 (2010).

[3] Van Loon, A. F. Hydrological drought explained. *WIREs Water* **2**, 359–392 (2015).

[7] UN-WATER. *The United Nations World Water Development Report 2018: Nature-Based Solutions for Water* (UNESCO: Paris, France, 2018).

[8] Ministry of Environment of Peru. *Ley No. 30215 De Mecanismos De Retribución Por Servicios Ecosistémicos – Law No. 30215 on Reward Mechanisms for Ecosystem Services* (El Peruano: Lima, Peru, 2014).

[10] Grainger, S. et al. The development and intersection of highland-coastal scale frames: a case study of water governance in central Peru. J. Environ. Pol. Plan. https://doi.org/10.1080/1523908X.2019.1566057 (2019).

[11] Ávila, J. *El Sistema de Infiltración Hídrica para el Mamanteo de Huamantanga – The Water Infiltration System for Huamantanga's Mamanteo* (Alternativa NGO: Huamantanga, Peru, 2012).

[12] Apaza, D., Arroyo, R., & Alcencastre, A. *Las Amunas de Huarochirí, Recarga de Acuíferos en los Andes – The Amunas of Huarochirí, Aquifer Recharge in the Andes* (Gestión Social del Agua y Ambiente en Cuencas – GSAAC: Lima, Peru, 2006).

[18] Pulido-Bosch, A. & Ben Sbih, Y. Centuries of artificial recharge on the southern edge of the Sierra Nevada (Granada, Spain). *Environ. Geol.* **26**, 57–63 (1995).

[22] Vogl, A. L. et al. (2017) Mainstreaming investments in watershed services to enhance water security: Barriers and opportunities. *Environ. Sci. Policy* **75**, 19–27 (2017).

[23] Manz, B. et al. High-resolution satellite-gauge merged precipitation climatologies of the Tropical Andes. *J. Geophys. Res. Atmos.* **121**, 1190–1207 (2016).

[30] Ochoa-Tocachi, B. F., Buytaert, W. & De Bièvre, B. Regionalization of land-use impacts on streamflow using a network of paired catchments. *Water Resour. Res.* **52**, 6710–6729 (2016).

[31] Bonnesoeur, V. et al. Impacts of forests and forestation on hydrological services in the Andes: A systematic review. *For. Ecol. Manag.* **433**, 569–584 (2019).

[36] Gammie, G. & De Bièvre, B. *Assessing Green Interventions for the Water Supply of Lima, Peru* (Forest Trends: Washington DC, USA, 2015).

[37] Vega-Jácome, F., Lavado-Casimiro, W. & Felipe-Obando, O. Assessing hydrological changes in a regulated river system over the last 90 years in Rimac Basin (Peru). *Theor. Appl. Climatol.* **132**, 347–362 (2018).

[38] Gutiérrez, O. F. *Huamantanga: Tierra Fecunda, Heroica y Legendaria – Huamantanga: Fertile, Heroic, and Legendary Land* (Orlando Francisco Gutiérrez Reymundo: Lima, Peru, 2018).

[39] Ministry of Agriculture of Peru. *Rumbo a un Programa Nacional de Siembra y Cosecha de Agua: Aportes y Reflexiones Desde la Práctica - Towards a National Programme of Water Harvesting: Contributions and Insights From the Practice* (Ministerio de Agricultura y Riego del Perú, Viceministerio de Políticas Agrarias: Lima, Peru, 2016).

[40] Ochoa-Tocachi, B. F. et al. Impacts of land use on the hydrological response of tropical Andean catchments. *Hydrol. Process.* **30**, 4074–4089 (2016).

[45] Hommes, L. & Boelens R. From natural flow to 'working river': Hydropower development, modernity and socio-territorial transformations in Lima's Rímac Watershed. *J. Hist. Geogr.* **62**, 85–95 (2018).

[46] Welch, L. A., & Allen, D. M. Consistency of groundwater flow patterns in mountainous topography: Implications for valley bottom water replenishment and for defining groundwater flow boundaries. *Water Resour. Res.* **48**, W05526 (2012).

[48] Ministry of Housing, Construction, and Sanitation of Peru. Ley No. 30045 De Modernización De Los Servicios De Saneamiento – Law No. 30045 on Modernisation of Sanitation Services (El Peruano: Lima, Peru, 2013).

[57] Ochoa-Tocachi, B. F. et al. High-resolution hydrometeorological data from a network of headwater catchments in the tropical Andes. *Sci. Data* **5**, 180080 (2018).

[62] Kieser, M. S. *Restoration of Amunas: Quantifying Potential Baseflow Improvements* (Forest Trends: Lima, Peru, 2014).

[63] U.S. Geological Survey. *Shuttle Radar Topography Mission (SRTM) 1 Arc-Second Global: SRTM1S13W077V3* (U.S. Geological Survey (USGS) Earth Resources Observation and Science (EROS) Center: Sioux Falls, SD, USA, 2014)

[64] Van Loon, A. F., Laaha, G. Hydrological drought severity explained by climate and catchment characteristics. *J. Hydrol.* **526**, 3–14 (2015).

[65] Beyene, B. S., Van Loon, A. F., Van Lanen, H. A. J. & Torfs, P. J. J. F. Investigation of variable threshold level approaches for hydrological drought identification. *Hydrol. Earth Syst. Sci. Discuss.* **11**, 12765–12797 (2014).

[66] Ochoa-Tocachi, B. F. Computer code for data processing and simulation of pre-Inca infiltration enhancement systems (mamanteo and amunas). *GitHub* https://github.com/topicster/mamanteo (2019).